

# Impact of Pulsar SAX J1748.9-2021 Observations on $f(\mathcal{Q}, \mathbb{T})$ Gravity

M. Sharif<sup>1,2\*</sup> and Iqra Ibrar<sup>1†</sup>

<sup>1</sup>Department of Mathematics and Statistics, The University of Lahore,  
1-KM Defence Road Lahore-54000, Pakistan.

<sup>2</sup> Research Center of Astrophysics and Cosmology, Khazar University,  
Baku, AZ1096, 41 Mehseti Street, Azerbaijan.

## Abstract

The main objective of this study is to investigate the viability and stability of a pulsar filled with anisotropic matter in  $f(\mathcal{Q}, \mathbb{T})$  gravity, where  $\mathcal{Q}$  represents non-metricity and  $\mathbb{T}$  is the trace of the energy-momentum tensor. In this context, we employ non-singular solution and a particular model of this gravity. We use junction conditions to evaluate unknown constants in the metric coefficients. Observations from the pulsar SAX J1748.9-2021 star are employed to validate the model, producing stable configurations that address both geometric and physical characteristics. This framework establishes relationships between various physical quantities, including fluid parameters, anisotropy, mass-radius relation, redshift, the Zeldovich condition, energy conditions, causality conditions, adiabatic index, Tolman-Oppenheimer-Volkoff equation, the equation of state parameter, and compactness. Our findings confirm the viability and stability of the proposed pulsar star in this theoretical framework.

**Keywords:** Pulsar;  $f(\mathcal{Q}, \mathbb{T})$  gravity; Stellar configuration.

**PACS:** 97.60.Gb; 04.50.Kd; 97.10.-q.

---

\*msharif.math@pu.edu.pk

†iqraibrar26@gmail.com

# 1 Introduction

General relativity (GR), proposed by Albert Einstein, is one of the most groundbreaking scientific achievements of the 20th century and serves as a cornerstone of modern physics. It provides a comprehensive framework to understand the evolution of the universe and its hidden mysteries. Recent advancements in cosmology have introduced innovative methods to study the universe accelerated expansion, supported by observational evidence such as redshift supernova observations [1], large-scale structures [2] and variations in cosmic microwave background radiation [3]. This rapid expansion is attributed to dark energy (DE), an unknown force responsible for approximately 68% of the universe total energy. While GR provides significant insights into this phenomenon through the inclusion of cosmological constant, it also presents challenges like fine-tuning and the coincidence problem. To address these limitations, modified gravity theories have been proposed, which expand on GR and offer explanation for late-time cosmic evolution and the accelerated expansion [4]. These theories align with GR in weak-field conditions but show notable deviations in strong gravitational fields. Compact astrophysical objects such as neutron stars, which exist in these extreme gravitational regimes, provide ideal environments to test the predictions of these modified theories and uncover phenomena unexplained by GR. Thus, while GR remains a fundamental pillar validated by extensive observations, modified theories open promising pathways for advancing our understanding of stellar astrophysics and cosmology.

One way to extend GR is by adopting broader geometric frameworks rather than Riemannian metric space. These new frameworks have the potential to elucidate the gravitational field and accurately describe the behavior of matter on vast cosmic scales. Weyl [5] developed a more general geometry than Riemannian space, aiming to unify fundamental forces within a single geometric structure. A fundamental concept in Riemannian geometry is the Levi-Civita connection, which enables the comparison of vectors by their length. Weyl implemented a connection for parallel transport that disregards information about the length of vectors. He added another connection called the length connection, which adjusts the conformal factor instead of the direction of vector transport. The theory claims that the covariant divergence of the metric tensor is non-zero, introducing the concept of non-metricity. He correlated the length connection with the electromagnetic potential and applied it to physical context.

The torsion and non-metricity scalars are mathematical quantities that emerge in modified theories incorporating non-Riemannian geometry. The  $f(\mathbb{T})$  gravity, a modified version of GR uses torsion to describe gravitational interactions. Nester and Yo [6] investigated teleparallel geometry characterized by zero curvature and torsion, but with a non-metricity included. This framework is known as symmetric teleparallel equivalent of GR (STG) and its extension is referred to as  $f(\mathcal{Q})$  gravity [7]. Lazkoz et al. [8] investigated the constraints of  $f(\mathcal{Q})$  theory using a polynomial redshift function. The energy conditions for two distinct  $f(\mathcal{Q})$  gravity models have been analyzed in [9]. Shekh [10] examined the dynamics of a DE model within this framework. Lin and Zhai [11] investigated the impact of the theory on the internal and external structures of compact stars by analyzing spherically symmetric solutions. Frusciante [12] proposed a model in  $f(\mathcal{Q})$  gravity that aligns with  $\Lambda$  cold dark matter (CDM) on a large scale while exhibiting distinct variations at smaller scales, offering measurable predictions. Dimakis et al. [14] studied the universe evolution both with and without a cosmological constant, as well as exploring the implications of phantom DE. Sokoliuk et al. [15] utilized the Pantheon dataset to explore cosmic evolution under  $f(\mathcal{Q})$  gravity. Bhar and Pretel [16] focused on compact stars and DE stars using the singularity-free Tolman-Kuchowicz metric, investigating quark stars by calculating their mass and radius based on specific equations of state (EoS). The pulsar SAX J1808.4-3658 was instrumental in analyzing the physical properties of DE stars, including their stability and causality conditions. Recent studies [17] have extensively explored various geometric and physical aspects of  $f(\mathcal{Q})$  gravity, providing valuable insights into the theory's versatility. Sharif and Ajmal [18] explored the characteristics of generalized ghost DE in  $f(\mathcal{Q})$  theory, while Sharif et al. [19] explored the concept of a cosmological bounce.

Xu et al. [20] extended the  $f(\mathcal{Q})$  theory by incorporating the trace of the energy-momentum tensor (EMT) into the functional action, resulting in the  $f(\mathcal{Q}, \mathbb{T})$  gravity. This theory establishes a specific connection between the trace of the EMT and non-metricity. This coupling offers a unified approach to gravitational phenomena, enabling  $f(\mathcal{Q}, \mathbb{T})$  gravity to explain both early-time inflation and late-time cosmic acceleration without requiring exotic DE. By modifying spacetime geometry itself, the theory naturally accounts for cosmic acceleration, incorporating matter density and pressure effects through  $\mathbb{T}$ . Unlike other modified theories of gravity that rely on additional fields or excessive fine-tuning,  $f(\mathcal{Q}, \mathbb{T})$  gravity enhances the flexibility of cosmological modeling. It fits observational data effectively while

predicting large-scale cosmic behavior. Additionally, its second-order field equations simplify calculations, making it practical for theoretical and computational studies. These advantages position  $f(\mathcal{Q}, \mathbb{T})$  gravity as a promising alternative framework for advancing cosmological understanding, though further research is necessary to establish its validity as a comprehensive model of the universe dynamics.

The motivation for studying this theory includes exploring its theoretical implications, checking its consistency with observational data and understanding its importance in cosmological applications. Arora et al. [21] examined the potential of this theory to explain the cosmic late-time acceleration without the necessity of additional DE forms. Bhattacharjee [22] investigated gravitational baryogenesis in this gravity, finding that it can significantly enhance baryon to entropy ratio. Godani and Samanta [23] explored  $f(\mathcal{Q}, \mathbb{T})$  gravity through a non-linear model, deriving cosmological implications consistent with supernova data and the  $\Lambda$ CDM model. Agrawal et al. [24] examined an extension of STG concerning late-time cosmic acceleration. Their work derives dynamical parameters and validate non-singular matter bounce models through energy conditions and stability analysis. Shiravand et al. [25] investigated cosmological inflation within  $f(\mathcal{Q}, \mathbb{T})$  gravity, deriving modified slow-roll parameters and spectral indices. Their findings demonstrate alignment with Planck 2018 observational data by appropriately constraining free parameters. Tayde et al. [28] analyzed the potential for wormholes within the framework of  $f(\mathcal{Q}, \mathbb{T})$  gravity. Recent studies underline the versatility of  $f(\mathcal{Q}, \mathbb{T})$  in addressing cosmological and astrophysical problems [30]-[37].

When a star runs out of nuclear fuel, it loses pressure, collapses and forms new dense stars called compact stars. Baade and Zwicky [38] proposed that compact stars are formed as a result of supernovae, a theory supported by the discovery of pulsars [39]. Pulsars are neutron stars that rotate and possess strong magnetic field emitting the beams of electromagnetic radiation. Examples like the pulsar star SAX J1748.9-2021 (PS) are crucial for understanding neutron star physics, accretion processes, and matter behavior in extreme gravitational and magnetic fields. They also offer powerful insights into binary system evolution and the final stages of stellar life cycles. In 1998, a sudden outburst led to the first observation of the neutron star, PS in a dense star cluster. Following this discovery, scientists identified its visible and inactive forms [40]. In 2001 [41], 2005 [42] and 2010 [43], more outbursts occurred, during which several X-ray bursts were detected. Sixteen of these bursts observed with the Rossi X-ray timing explorer that showed the signs

of powerful explosions on the neutron stars surface.

The fascinating properties and structures of neutron stars have attracted considerable attention. Mak and Harko [44] studied the stability of pulsars by looking at energy limits and their stable state through the speed of sound. Kramer et al. [45] highlighted the significance and potential of the double pulsar system PSR J0737-3039A/B for performing precise tests of GR and modified theories. Sharma et al. [46] analyzed the 2017 outburst of PS using the AstroSat telescope and discovered key spectral and timing characteristics of the pulsar, including an average spin frequency of 442.361098 Hz. Recently, the impacts of  $f(\mathcal{R})$  and  $f(\mathcal{R}, \mathbb{T})$  theories on PS are discussed [47, 48].

This paper aims to investigate the viable characteristics of anisotropic PS within the framework of  $f(\mathcal{Q}, \mathbb{T})$  theory. The structure of this paper is as follows. Section 2 provides a comprehensive overview of  $f(\mathcal{Q}, \mathbb{T})$  theory and its field equations. In section 3, the field equations for a specific model  $f(\mathcal{Q}, \mathbb{T})$  and the Krori-Barua (KB) ansatz are employed. We use matching conditions to determine the unknown constants in the KB ansatz. In sections 4 and 5, we utilize observational data of PS to find density, radial and tangential pressures, anisotropy, mass-radius relation, redshift, the Zel-dovich condition, energy conditions, causality condition, adiabatic index and Tolman-Oppenheimer-Volkoff (TOV) equation, EoS parameter and compactness. We also assess stability of the model based on these physical constraints. The final section presents our main results.

## 2 Formalism of $f(\mathcal{Q}, \mathbb{T})$ Theory

This section presents the basic framework of the modified  $f(\mathcal{Q}, \mathbb{T})$  theory, employing the variational principle to derive the field equations. Weyl [5] proposed an extension of Riemannian geometry as a mathematical basis for explaining gravitation in the context of GR. This modification introduces a new vector field,  $\Psi^\alpha$ , which delineates geometric properties of the Weyl geometry. Weyl theory suggests that a vector field shares similar mathematical properties with electromagnetic potentials in physics, highlighting a strong connection between gravitational and electromagnetic forces [49]. In Weyl geometry, when a vector of length  $y$  is transported along an infinitesimal path  $\delta x^\xi$ , its new length is given by  $\delta y = y\Psi_\xi \delta x^\xi$ .

The connection in Weyl-Cartan space can be represented as

$$\hat{\Gamma}_{\xi\varrho}^\lambda = \Gamma_{\xi\varrho}^\lambda + C_{\xi\varrho}^\lambda + L_{\xi\varrho}^\lambda, \quad (1)$$

where  $\Gamma_{\xi\varrho}^\lambda$  denotes the usual Christoffel symbol,  $C_{\xi\varrho}^\lambda$  represents the contortion tensor,  $L_{\xi\varrho}^\lambda$  indicates the disformation tensor. The contortion tensor can be derived

$$C_{\xi\varrho}^\lambda = \hat{\Gamma}_{[\xi\varrho]}^\lambda + g^{\lambda\phi} g_{\xi\kappa} \hat{\Gamma}_{[\varrho\phi]}^\kappa + g^{\lambda\phi} g_{\varrho\kappa} \hat{\Gamma}_{[\xi\phi]}^\kappa. \quad (2)$$

The disformation tensor can be obtained as

$$L_{\xi\varrho}^\lambda = \frac{1}{2} g^{\lambda\phi} (\mathcal{Q}_{\varrho\xi\phi} + \mathcal{Q}_{\xi\varrho\phi} - \mathcal{Q}_{\lambda\xi\varrho}), \quad (3)$$

where

$$\mathcal{Q}_{\lambda\xi\varrho} = \nabla_\lambda g_{\xi\varrho}. \quad (4)$$

The Weyl-Cartan torsion is described as

$$T_{\xi\varrho}^\lambda = \frac{1}{2} (\hat{\Gamma}_{\xi\varrho}^\lambda - \hat{\Gamma}_{\varrho\xi}^\lambda). \quad (5)$$

The connection is defined by the disformation tensor as

$$\Gamma_{\xi\varrho}^\lambda = -L_{\xi\varrho}^\lambda. \quad (6)$$

The gravitational action in a non-covariant form is expressed as [50]

$$S = \frac{1}{2\kappa} \int g^{\xi\varrho} (\Gamma_{\phi\xi}^\rho \Gamma_{\varrho\rho}^\phi - \Gamma_{\phi\rho}^\rho \Gamma_{\xi\varrho}^\phi) \sqrt{-g} d^4x, \quad (7)$$

where  $\kappa$  signifies the coupling constant, which is chosen to be one,  $g$  indicates determinant of the metric tensor. Utilizing the relation (6), the action integral becomes

$$S = -\frac{1}{2} \int g^{\xi\varrho} (L_{\phi\xi}^\rho L_{\varrho\rho}^\phi - L_{\phi\rho}^\rho L_{\xi\varrho}^\phi) \sqrt{-g} d^4x. \quad (8)$$

This is known as the action of STG and is equivalent to the Einstein-Hilbert action. There are several important differences between the two gravitational paradigms. One notable feature is that the disappearance of the curvature tensor in STG results in the system appearing as a uniformly flat structure. Moreover, gravitational effects are attributed to variations in the length of a vector, rather than to the rotation of the angle between two vectors during parallel transport.

Next, we examine an extension of the STG Lagrangian given by Eq.(8), which is formulated as follows

$$S = \int \left[ \frac{1}{2} f(\mathcal{Q}) + L_m \right] \sqrt{-g} d^4x, \quad (9)$$

where  $L_m$  represents the matter Lagrangian. Now, we extend this gravitational Lagrangian by adding the trace of the EMT to the functional action as follows

$$S = \int \left[ \frac{1}{2} f(\mathcal{Q}, \mathbb{T}) + L_m \right] \sqrt{-g} d^4x. \quad (10)$$

Moreover

$$\mathcal{Q} = -g^{\xi\varrho} (L_{\mu\xi}^\rho L_{\varrho\rho}^\mu - L_{\mu\rho}^\rho L_{\xi\varrho}^\mu), \quad (11)$$

where

$$L_{\mu\varpi}^\rho = -\frac{1}{2} g^{\rho\lambda} (\nabla_\varpi g_{\mu\lambda} + \nabla_\mu g_{\lambda\varpi} - \nabla_\lambda g_{\mu\varpi}). \quad (12)$$

The traces of the non-metricity tensor are defined by the following expressions

$$\mathcal{Q}_\rho = \mathcal{Q}_\rho^\xi{}_\xi, \quad \tilde{\mathcal{Q}}_\rho = \mathcal{Q}_{\rho\xi}^\xi. \quad (13)$$

The superpotential with respect to  $\mathcal{Q}$  is expressed as

$$P_{\xi\varrho}^\rho = -\frac{1}{2} L_{\xi\varrho}^\rho + \frac{1}{4} (\mathcal{Q}^\rho - \tilde{\mathcal{Q}}^\rho) g_{\xi\varrho} - \frac{1}{4} \delta_{[\xi\varrho]}^\rho. \quad (14)$$

Furthermore, the expression for  $\mathcal{Q}$  obtained through the superpotential can be written as follows [18]

$$\mathcal{Q} = -\mathcal{Q}_{\rho\xi\varrho} P^{\rho\xi\varrho} = -\frac{1}{4} (-\mathcal{Q}^{\rho\xi\varrho} \mathcal{Q}_{\rho\varrho\xi} + 2\mathcal{Q}^{\rho\varrho\xi} \mathcal{Q}_{\xi\rho\varrho} - 2\mathcal{Q}^\varrho \tilde{\mathcal{Q}}_\varrho + \mathcal{Q}^\varrho \mathcal{Q}_\varrho). \quad (15)$$

The field equations are obtained by taking the variation of  $S$  with respect to the metric tensor and equating it to zero as follows

$$\begin{aligned} \delta S = 0 &= \int \frac{1}{2} \delta[f(\mathcal{Q}, \mathbb{T}) \sqrt{-g}] + \delta[L_m \sqrt{-g}] d^4x \\ 0 &= \int \frac{1}{2} \left( \frac{-1}{2} f g_{\xi\varrho} \sqrt{-g} \delta g^{\xi\varrho} + f_{\mathcal{Q}} \sqrt{-g} \delta \mathcal{Q} + f_{\mathbb{T}} \sqrt{-g} \delta \mathbb{T} \right) - \frac{1}{2} \mathbb{T}_{\xi\varrho} \sqrt{-g} \delta g^{\xi\varrho} d^4x. \end{aligned} \quad (16)$$

Additionally, we define

$$\mathbb{T}_{\xi\varrho} = \frac{-2}{\sqrt{-g}} \frac{\delta(\sqrt{-g}L_m)}{\delta g^{\xi\varrho}}, \quad \Theta_{\xi\varrho} = g^{\rho\mu} \frac{\delta \mathbb{T}_{\rho\mu}}{\delta g^{\xi\varrho}}, \quad (17)$$

which implies that  $\delta \mathbb{T} = \delta(\mathbb{T}_{\xi\varrho} g^{\xi\varrho}) = (\mathbb{T}_{\xi\varrho} + \Theta_{\xi\varrho}) \delta g^{\xi\varrho}$ . Inserting the aforementioned factors in Eq.(16), we have

$$\begin{aligned} \delta S = 0 &= \int \frac{1}{2} \left\{ \frac{-1}{2} f g_{\xi\varrho} \sqrt{-g} \delta g^{\xi\varrho} + f_{\mathbb{T}} (\mathbb{T}_{\xi\varrho} + \Theta_{\xi\varrho}) \sqrt{-g} \delta g^{\xi\varrho} \right. \\ &\quad - f_{\mathcal{Q}} \sqrt{-g} (P_{\xi\rho\mu} \mathcal{Q}_{\varrho}{}^{\rho\mu} - 2 \mathcal{Q}^{\rho\varrho}{}_{\xi} P_{\rho\mu\varrho}) \delta g^{\xi\varrho} + 2 f_{\mathcal{Q}} \sqrt{-g} P_{\rho\xi\varrho} \nabla^{\rho} \delta g^{\xi\varrho} \\ &\quad \left. + 2 f_{\mathcal{Q}} \sqrt{-g} P_{\rho\xi\varrho} \nabla^{\rho} \delta g^{\xi\varrho} \right\} - \frac{1}{2} \mathbb{T}_{\xi\varrho} \sqrt{-g} \delta g^{\xi\varrho} d^4x. \end{aligned} \quad (18)$$

When integrating the term  $2 f_{\mathcal{Q}} \sqrt{-g} P_{\rho\xi\varrho} \nabla^{\rho} \delta g^{\xi\varrho}$  and applying the boundary conditions, the resulting expression is  $-2 \nabla^{\rho} (f_{\mathcal{Q}} \sqrt{-g} P_{\rho\xi\varrho}) \delta g^{\xi\varrho}$ . The partial derivatives with respect to  $\mathcal{Q}$  and  $\mathbb{T}$  are represented by  $f_{\mathcal{Q}}$  and  $f_{\mathbb{T}}$ , respectively. Finally, we can write the field equations as follows

$$\begin{aligned} \mathbb{T}_{\xi\varrho} &= \frac{-2}{\sqrt{-g}} \nabla_{\rho} (f_{\mathcal{Q}} \sqrt{-g} P_{\xi\varrho}^{\rho}) - \frac{1}{2} f g_{\xi\varrho} + f_{\mathbb{T}} (\mathbb{T}_{\xi\varrho} + \Theta_{\xi\varrho}) \\ &\quad - f_{\mathcal{Q}} (P_{\xi\rho\mu} \mathcal{Q}_{\varrho}{}^{\rho\mu} - 2 \mathcal{Q}^{\rho\mu}{}_{\xi} P_{\rho\mu\varrho}). \end{aligned} \quad (19)$$

To study the internal structure of a star in equilibrium, we examine a spherically symmetric system. The line element is given as

$$ds^2 = -e^{\alpha(r)} dt^2 + e^{\beta(r)} dr^2 + r^2 (d\theta^2 + \sin^2 \theta d\phi^2). \quad (20)$$

We consider the stellar matter distribution to be an anisotropic, which can be characterized by

$$\mathbb{T}_{\xi\varrho} = (\rho + P_t) u_{\xi} u_{\varrho} + P_t g_{\xi\varrho} - \sigma k_{\xi} k_{\varrho}, \quad (21)$$

here,  $u_{\xi}$  and  $u_{\varrho}$  represent the four-velocity of the fluid, adhering to the normalization condition  $u^{\xi} u_{\xi} = -1$ . Additionally,  $k_{\xi}$  is a unit radial four-vector that satisfies the condition  $k^{\xi} k_{\xi} = 1$ . In this context, the energy density is  $\rho$ , the tangential pressure is  $P_t$ , the radial pressure is  $P_r$  and the anisotropy factor is  $\sigma$  defined as  $(P_t - P_r)$ . Based on the given metric, we can write  $u^{\xi}$  as  $e^{-\alpha} \delta_t^{\xi}$ , and  $k^{\xi}$  as  $e^{-\beta} \delta_r^{\xi}$ . Thus, the trace of the EMT in Eq.(20) can be represented as

$$\tilde{\mathbb{T}} = -\rho + 3P_r + 2\sigma. \quad (22)$$



Taking the divergence of Eq.(21) results in the conservation law for energy and momentum, expressed as

$$\nabla_e \tilde{\mathbb{T}}_1^e = (\rho + P_r)\alpha' + P_r' - \frac{1}{r}\sigma, \quad (23)$$

where prime is the derivative with respect to  $r$ . The non-zero parts of the field equations (19) are

$$\begin{aligned} \rho = \frac{1}{2r^2 e^{\beta(r)}} & \left[ f_{\mathcal{Q}}((e^{\beta(r)} - 1)(r\alpha'(r) + 2) + r(e^{\beta(r)} + 1)\beta'(r)) \right. \\ & \left. + 2f_{\mathcal{Q}\mathcal{Q}}r(e^{\beta(r)} - 1)Q'(r) + fr^2 e^{\beta(r)} \right] - \frac{1}{3}f_{\mathbb{T}}(P_r + 2P_t + 3\rho), \end{aligned} \quad (24)$$

$$\begin{aligned} P_r = \frac{1}{2r^2 e^{\beta(r)}} & \left[ f_{\mathcal{Q}}((e^{\beta(r)} - 1)(r\alpha'(r) + r\beta'(r) + 2) - 2r\alpha'(r)) \right. \\ & \left. + 2f_{\mathcal{Q}\mathcal{Q}}r(e^{\beta(r)} - 1)Q'(r) \right] + \frac{2}{3}f_{\mathbb{T}}(P_t - P_r) + fr^2 e^{\beta(r)}, \end{aligned} \quad (25)$$

$$\begin{aligned} P_t = \frac{1}{3}f_{\mathbb{T}}(P_r - P_t) - \frac{1}{4re^{\beta(r)}} & \left[ f_{\mathcal{Q}}(-2r\alpha''(r) + \beta'(r)(r\alpha'(r) + 2e^{\beta(r)})) \right. \\ & \left. + 2(e^{\beta(r)} - 2)\alpha'(r) - r\alpha'(r)^2 - 2f_{\mathcal{Q}\mathcal{Q}}rQ'(r)\alpha'(r) + 2fre^{\beta(r)} \right]. \end{aligned} \quad (26)$$

### 3 The $f(\mathcal{Q}, \mathbb{T})$ Gravity Model

We now examine the influence of  $f(\mathcal{Q}, \mathbb{T})$  on the geometry of PS. For this purpose, we utilize the specific model of  $f(\mathcal{Q}, \mathbb{T})$  as [51].

$$f(\mathcal{Q}, \mathbb{T}) = \zeta \mathcal{Q} + \eta \mathbb{T}, \quad (27)$$

where  $\zeta$  and  $\eta$  are arbitrary constants with  $f_{\mathcal{Q}} = \zeta$ ,  $f_{\mathcal{Q}\mathcal{Q}} = 0$ ,  $f_{\mathbb{T}} = \eta$ ,  $f_{\mathbb{T}\mathbb{T}} = 0$ . This cosmological model is extensively employed in the literature [52]. Substituting these values into Eqs.(24)-(26), we obtain

$$\begin{aligned} \rho = \frac{1}{2r^2(\eta(-8\eta + 2(4\eta + 3)r^2 e^{\beta(r)} - 15) - 6)} & \left[ \zeta e^{-\beta(r)}(r(\eta\alpha'(r)((e^{\beta(r)} - 1) \right. \\ & \times (2r^2 e^{\beta(r)} - 1) + r\beta'(r)) + (\eta(e^{\beta(r)}(2r^2(e^{\beta(r)} + 5) - 1) - 9) - 12)\beta'(r) \\ & \left. - 2\eta r\alpha''(r) + \eta(-r)\alpha'(r)^2) + 2(e^{\beta(r)} - 1)(\eta(6r^2 e^{\beta(r)} - 7) - 6)) \right], \end{aligned} \quad (28)$$

$$\begin{aligned}
P_r = & \frac{1}{2(\eta+1)r^2(\eta(-8\eta+2(4\eta+3)r^2e^{\beta(r)}-15)-6)} \left[ \zeta e^{-\beta(r)} (r(-2\eta r\alpha''(r) \right. \\
& \times (3\eta+2(4\eta+3)r^2e^{\beta(r)}+2) + \alpha'(r)(\eta(27\eta+47) + \eta r(3\eta+2(4\eta+3)r^2 \\
& \times e^{\beta(r)}+2)\beta'(r) + 2(\eta+1)(11\eta+6)r^2e^{2\beta(r)} - e^{\beta(r)}((\eta+1)(11\eta+6) \\
& + 2(\eta(19\eta+23)+6)r^2) + 18) + \eta(-r)\alpha'(r)^2(3\eta+2(4\eta+3)r^2e^{\beta(r)}+2) \\
& + (\eta(13\eta+21) + 2(\eta+1)(11\eta+6)r^2e^{2\beta(r)} - e^{\beta(r)}((\eta+1)(11\eta+6) + 2 \\
& \times (\eta+2)(\eta+3)r^2) + 6)\beta'(r)) + 2(e^{\beta(r)}-1)(\eta(-13\eta+2(\eta+3)r^2 \\
& \times e^{\beta(r)}-17)-6)) \left. \right], \tag{29}
\end{aligned}$$

$$\begin{aligned}
P_t = & \frac{1}{4(\eta+1)r^2(\eta(-8\eta+2(4\eta+3)r^2e^{\beta(r)}-15)-6)} \left[ \zeta e^{-\beta(r)} (r(2(r\alpha''(r) \right. \\
& \times (\eta(-6\eta+2(4\eta+3)r^2e^{\beta(r)}-13)-6) + (\eta(\eta+e^{\beta(r)}(\eta-2r^2(\eta+(\eta+1) \\
& \times e^{\beta(r)}+2)+1)+6)\beta'(r)) + \alpha'(r)(r(\eta(6\eta-2(4\eta+3)r^2e^{\beta(r)}+13) \\
& + 6)\beta'(r) + 2\eta(-9\eta+e^{\beta(r)}(\eta-2r^2(-5\eta+(\eta+1)e^{\beta(r)}-4)+1)-16) \\
& - 12) + r\alpha'(r)^2(\eta(-6\eta+2(4\eta+3)r^2e^{\beta(r)}-13)-6)) + 4\eta(e^{\beta(r)}-1) \\
& \times (\eta(2r^2e^{\beta(r)}-1)-2)) \left. \right]. \tag{30}
\end{aligned}$$

We make some reasonable assumptions about the metric potentials  $\alpha(r)$  and  $\beta(r)$  to study stellar evolution. We use the KB spacetime to investigate stellar models within the framework of modified gravity theory.

### 3.1 The Krori-Barua Metric Potentials

This is a well-known ansatz used in GR to model the interior of stars. It provides a specific form of the metric potentials that satisfy the Einstein field equations under certain conditions. The KB metric is particularly useful for studying the structure and properties of highly dense astrophysical objects such as PS. The metric potentials of KB are defined as [53]

$$\alpha(r) = A_1 \left( \frac{r}{R} \right)^2 + a_1, \quad \beta(r) = a \left( \frac{r}{R} \right)^2, \tag{31}$$

where  $R$  represents the radius of the star and  $A_1, a_1$  and  $a$  are arbitrary constants and can be found by using junction conditions. It helps in under-

standing how different theoretical frameworks such as  $f(\mathcal{Q}, \mathbb{T})$  gravity affect the properties of these stars.

The KB metric is particularly advantageous within the  $f(\mathcal{Q}, \mathbb{T})$  gravity framework because of its smooth and non-singular behavior at both the stellar core  $r = 0$  and surface  $r = R$ . This ensures that physical parameters, such as density and pressure, remain well-behaved throughout the stellar interior, avoiding singularities that could compromise the model physical validity. Additionally, the KB metric is robust and flexible, making it adaptable to modified gravity frameworks like  $f(\mathcal{Q}, \mathbb{T})$ , where geometric modifications arise from non-metricity and the trace of the EMT. Its use is further justified by its ability to incorporate observational mass-radius constraints, such as those from PS, thereby bridging theoretical modeling with real-world astrophysical data.

### 3.2 Matching Conditions

Matching conditions are essential in the study of stellar structures and GR. These conditions ensure that the interior solution of a star, described by its matter distribution and gravitational field, smoothly connects with the exterior vacuum solution, typically represented by the Schwarzschild solution, given by

$$ds^2 = -\left(1 - \frac{2GM}{c^2 r}\right) c^2 dt^2 + \left(1 - \frac{2GM}{c^2 r}\right)^{-1} dr^2 + r^2(d\theta + \sin^2 \theta d\phi^2), \quad (32)$$

where  $M$  denotes the mass of the star,  $G$  is the gravitational constant and  $c$  is the speed of light. The continuity of the metric coefficients for the metrics (20) and (32) at the surface boundary ( $r = R$ ) results in

$$g_{tt} = e^{A_1 \left(\frac{r}{R}\right)^2 + a_1} = -\left(1 - \frac{2GM}{c^2 r}\right) c^2, \quad (33)$$

$$g_{rr} = e^{a \left(\frac{r}{R}\right)^2} = \left(1 - \frac{2GM}{c^2 r}\right)^{-1}. \quad (34)$$

Applying the matching conditions, we have

$$\alpha(r = R) = \ln(-u + 1), \quad \beta(r = R) = -\ln(-u + 1), \quad P_r(r = R) = 0, \quad (35)$$

where  $u$  denotes compactness, defined as

$$u = \frac{2GM}{c^2 R}, \quad (36)$$

Table 1: Physical quantities and their units used in the analysis.

Variable	Physical Meaning	Units
$\rho$	Density	$g/cm^3$
$P_r, P_t$	Radial/Tangential pressure	$dyn/cm^2$
$u$	Compactness ( $u = \frac{M}{R}$ )	Dimensionless
$v_r^2, v_t^2$	Squared sound speeds (Radial/Tangential)	Dimensionless
$Z_s$	Gravitational redshift	Dimensionless
$\Gamma$	Adiabatic index	Dimensionless

here, we use the gravitational units such that  $c = G = 1$ .

Having established the rationale for the KB metric, we now discuss the significance of the boundary condition  $P_r = 0$  at  $r = R$ . Physically, at the stellar surface, there is no external pressure acting on the star, as the surrounding region is a vacuum described by the Schwarzschild solution. This necessitates setting the  $P_r = 0$  at  $r = R$ , ensuring a smooth and natural transition between the star interior solution (with anisotropic matter) and the exterior vacuum solution. Mathematically, this condition guarantees the continuity of the metric coefficients  $g_{tt}$  and  $g_{rr}$  and their derivatives at the stellar boundary. Such continuity is essential for satisfying the junction conditions required in GR and its extensions, including  $f(Q, \mathbb{T})$  gravity. The absence of any pressure discontinuity eliminates non-physical behavior at the surface, which could otherwise destabilize the star.

The boundary condition,  $P_r = 0$ , also has a direct impact on the model stability and accuracy. It ensures hydrostatic equilibrium, where the outward pressure gradient balances the inward gravitational pull, preventing matter from escaping and maintaining structural stability. In terms of accuracy, this condition is critical for determining free parameters, such as the metric coefficients, which define the star internal structure. It enables the derivation of a physically realistic mass-radius relation and compactness, aligning the theoretical predictions with observational data like PS. Without these boundary conditions, the model would exhibit pressure inconsistencies, unstable behavior, and unrealistic predictions, ultimately undermining its physical validity. Table 1 ensures numerical consistency and address concerns regarding units that explicitly states all the physical quantities used in our analysis along with their corresponding units.

## 4 Stability Analysis from SAX J 1748.9-2021 Observations

In this section, we use observational data focusing on the mass and radius of PS within the framework of  $f(\mathcal{Q}, \mathbb{T})$  gravity. The observational data for PS was obtained from spectroscopic measurements during thermonuclear bursts, as reported in prior studies using the Rossi X-ray timing explorer. This dataset provides high-precision measurements of the pulsar's mass  $M = 1.81 \pm 0.3M_{\odot}$  and radius ( $R = 11.7 \pm 1.7$ )km, making this pulsar an ideal candidate for testing modified gravity models. The unique characteristics of this PS, such as its rapid spin frequency (442.361098)Hz and compact configuration, further justify its selection for this study. These properties offer an excellent opportunity to examine strong-field deviations from GR and validate the predictions of the  $f(\mathcal{Q}, \mathbb{T})$  framework. Additionally, we outline the criteria for selecting PS as the focus of our study, emphasizing the availability of accurate and reliable observational data that align well with the theoretical framework of  $f(\mathcal{Q}, \mathbb{T})$  gravity. To further strengthen the reliability of our results, we have conducted a systematic uncertainty analysis by propagating uncertainties in the observational data through the field equations.

### 4.1 Material Component

In the study of stellar models, key physical quantities such as  $\rho$ ,  $P_r$ ,  $P_t$  and anisotropy play crucial roles in determining the behavior and stability of the star. They provide insights into the internal structure and dynamics of the material component of the star. The quantities  $\rho$ ,  $P_r$  and  $P_t$  are derived from the model's field equations using a combination of analytical and numerical methods. Initially, the field equations are solved analytically and then mathematical software, such as Mathematica, is employed to obtain simplified expressions for these quantities. This approach helps us to manage the algebraic complexity effectively and derives the simplified forms of  $\rho$ ,  $P_r$  and  $P_t$ . Once these quantities are determined through the field equations, we have applied a linear model and utilized the KB metric to further simplify the equations. By following these steps, we have successfully derived the

following quantities

$$\begin{aligned} \rho = & \left[ \zeta e^{-\frac{ar^2}{R^2}} \left( -2A_1^2\eta r^4 + 2A_1a\eta r^4 + 2\eta r^2 R^2 e^{\frac{2ar^2}{R^2}} (r^2(A_1 + a) + 3R^2) \right. \right. \\ & - R^2 e^{\frac{ar^2}{R^2}} (\eta r^2(2r^2(A_1 - 5a) + A_1 + a) + R^2(\eta(6r^2 + 7) + 6)) - A_1 \\ & \times \eta r^2 R^2 - 9a\eta r^2 R^2 - 12ar^2 R^2 + 7\eta R^4 + 6R^4) \left. \right] \left[ r^2 R^4 (\eta(2(4\eta + 3)r^2 e^{\frac{ar^2}{R^2}} \right. \\ & \left. \left. - 8\eta - 15) - 6) \right]^{-1}, \end{aligned} \quad (37)$$

$$\begin{aligned} P_r = & \left[ \zeta e^{-\frac{ar^2}{R^2}} \left( \frac{1}{R^4} \left[ 2r^2 \left( -e^{\frac{ar^2}{R^2}} (4A_1^2\eta(4\eta + 3)r^4 + A_1(R^2((\eta + 1)(11\eta + 6) \right. \right. \right. \right. \\ & + 2(\eta(27\eta + 29) + 6)r^2) - 4a\eta(4\eta + 3)r^4) + aR^2((\eta + 1)(11\eta + 6) + 2 \\ & \times (\eta + 2)(\eta + 3)r^2)) - 6A_1^2\eta^2 r^2 - 4A_1^2\eta r^2 + 6A_1a\eta^2 r^2 + 4A_1a\eta r^2 + 2 \\ & \times (\eta + 1)(11\eta + 6)r^2 R^2(A_1 + a)e^{\frac{2ar^2}{R^2}} + 21A_1\eta^2 R^2 + 43A_1\eta R^2 + 18A_1 R^2 \\ & + 13a\eta^2 R^2 + a\eta R^2 + 6aR^2) \left. \right] + 2(e^{\frac{ar^2}{R^2}} - 1)(\eta(2(\eta + 3)r^2 e^{\frac{ar^2}{R^2}} - 13\eta)) \left. \right] \\ & \times \left[ 2(\eta + 1)r^2(\eta(2(4\eta + 3)r^2 e^{\frac{ar^2}{R^2}} - 8\eta - 15) - 6) \right]^{-1}, \end{aligned} \quad (38)$$

$$\begin{aligned} P_t = & \left[ \zeta e^{-\frac{ar^2}{R^2}} \left( A_1^2 r^4 (\eta(2(4\eta + 3)r^2 e^{\frac{ar^2}{R^2}} - 6\eta - 13) - 6) + A_1 r^2 (ar^2(\eta(-2 \right. \right. \\ & + (4\eta + 3)r^2 e^{\frac{ar^2}{R^2}} 6\eta + 13) + 6) + R^2(\eta(e^{\frac{ar^2}{R^2}}(2r^2(-(\eta + 1)e^{\frac{ar^2}{R^2}} + 9\eta + 7) \\ & + \eta + 1) - 15\eta - 29) - 12)) + R^2(ar^2(\eta(e^{\frac{ar^2}{R^2}}(2r^2(-(\eta + 1)e^{\frac{ar^2}{R^2}} - \eta - 2) \\ & + \eta + 1) + \eta + 6) + 6) + \eta R^2(e^{\frac{ar^2}{R^2}} - 1)(2\eta r^2 e^{\frac{ar^2}{R^2}} - \eta - 2))) \left. \right] \\ & \times \left[ r^2 R^4 (\eta(2(\eta + 1)(4\eta + 3)r^2 e^{\frac{ar^2}{R^2}} - \eta(8\eta + 23) - 21) - 6) \right]^{-1}. \end{aligned} \quad (39)$$

The constants are set as  $A_1 = 2$ ,  $a_1 = 0$ ,  $a = -2$  and various values of  $\zeta = 1, 1.04$  and  $1.08$ . Throughout the paper these values are applied consistently to derive and evaluate our equations and results. To further strengthen the reliability of our results, we performed a systematic uncertainty analysis by propagating the uncertainties in the radius through the field equations.

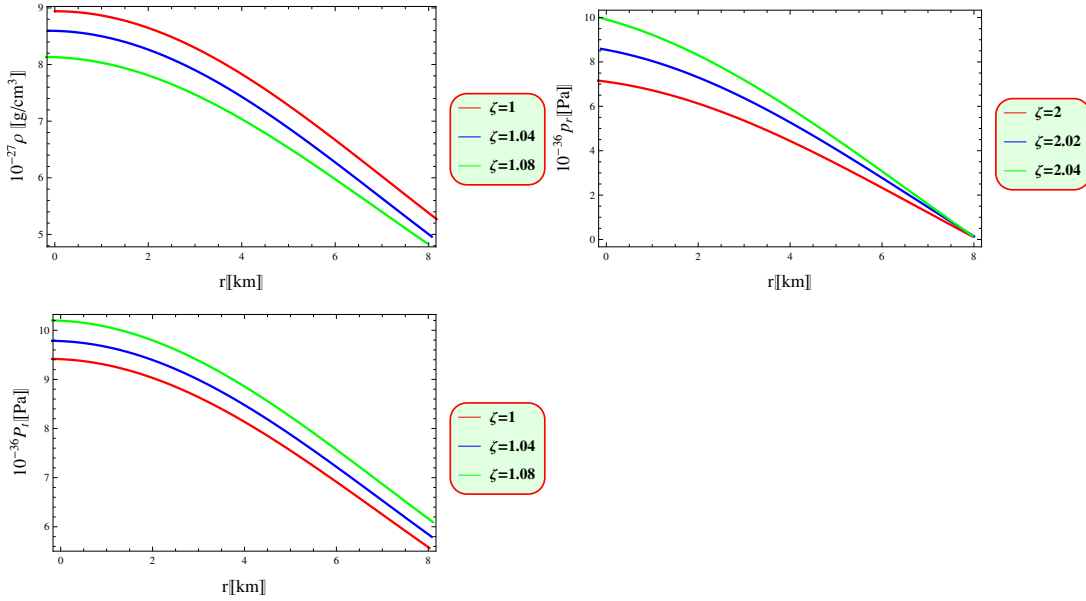


Figure 1: Plots of  $\rho$ ,  $P_r$ ,  $P_t$  versus  $r$ .

We have analyzed the impact of these uncertainties on key physical parameters, such as  $\rho$ ,  $P_r$ ,  $P_t$  and compactness. The results confirmed that these parameters remain stable and within physically expected bounds, validating the robustness of our model. Additionally, we have conducted a sensitivity analysis by varying the parameter  $\zeta$  and studying its effect on the results. We have observed a consistent increasing trend in the graphs for three different values of  $\zeta$ . The parameter values were carefully fixed to ensure smooth and physically consistent behavior in the graphs. Testing lower values, such as  $R = 10\text{km}$ , led to deviations from the expected behavior, reinforcing the choice of  $R = 13.4\text{km}$  for producing meaningful and consistent results. We have employed Mathematica for solving the field equations. Figure 1 presents the plots of  $\rho$ ,  $P_r$  and  $P_t$  as functions of  $r$ , showing that these physical characteristics are peak at the center and decrease outward indicating a highly compact profile for the proposed PS. Additionally, the  $P_r$  within PS consistently decreases as  $r$  increases.

Anisotropic  $\sigma$  pressure refers to the condition where the pressure within a material or system is not uniform in all directions. This directional dependence of pressure can significantly influence the behavior and stability of

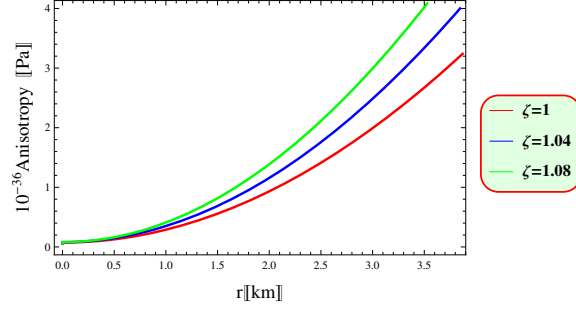


Figure 2: Plot of  $\sigma$  against  $r$ .

physical systems, such as stars, where anisotropic pressure can affect their structural integrity and evolution [56]. The anisotropy ( $\sigma = P_t - P_r$ ) leads to

$$\begin{aligned} \sigma = & \frac{1}{r^2 R^4 (\eta(2(\eta+1)(4\eta+3)r^2 e^{\frac{A_1 r^2}{R^2}} - \eta(8\eta+23) - 21) - 6)} \left[ \zeta e^{-\frac{A_1 r^2}{R^2}} (a^2 r^4 \right. \\ & \times (\eta(2(4\eta+3)r^2 e^{\frac{A_1 r^2}{R^2}} - 6\eta - 13) - 6) + a r^2 (A_1 r^2 (\eta(-2(4\eta+3)r^2 e^{\frac{A_1 r^2}{R^2}} \\ & + 6\eta + 13) + 6) + R^2 (\eta(e^{\frac{A_1 r^2}{R^2}} (2r^2 (- (\eta+1)e^{\frac{A_1 r^2}{R^2}} + 9\eta + 7) + \eta + 1) \\ & - 15\eta - 29) - 12)) + R^2 (A_1 r^2 (\eta(e^{\frac{A_1 r^2}{R^2}} (2r^2 (- (\eta+1)e^{\frac{A_1 r^2}{R^2}} - \eta - 2) \\ & + \eta + 1) + \eta + 6) + 6) + \eta R^2 (e^{\frac{A_1 r^2}{R^2}} - 1) (2\eta r^2 e^{\frac{A_1 r^2}{R^2}} - \eta - 2))) \Big] \\ & - \left( 2(\eta+1)r^2 (\eta(2(4\eta+3)r^2 e^{\frac{A_1 r^2}{R^2}} - 8\eta - 15) - 6) \right)^{-1} \left[ \zeta e^{-\frac{A_1 r^2}{R^2}} \left( \frac{1}{R^4} \right. \right. \\ & \times \left\{ 2r^2 \left( -e^{\frac{A_1 r^2}{R^2}} (4a^2 \eta(4\eta+3)r^4 + a(R^2((\eta+1)(11\eta+6) + 2(\eta(27\eta+29) \right. \right. \\ & + 6)r^2) - 4A_1 \eta(4\eta+3)r^4) + A_1 R^2((\eta+1)(11\eta+6) + 2(\eta+2)(\eta+3)r^2)) \right. \\ & - 6a^2 \eta^2 r^2 - 4a^2 \eta r^2 + 6aA_1 \eta^2 r^2 + 4aA_1 \eta r^2 + 2(\eta+1)(11\eta+6)r^2 R^2 (a + A_1) \\ & \times e^{\frac{2A_1 r^2}{R^2}} + 21a\eta^2 R^2 + 43a\eta R^2 + 18aR^2 + 13A_1 \eta^2 R^2 + 21A_1 \eta R^2 + 6A_1 R^2) \Big\} \\ & \left. \left. + 2 \left( e^{\frac{A_1 r^2}{R^2}} - 1 \right) \times (\eta(2(\eta+3)r^2 e^{\frac{A_1 r^2}{R^2}} - 13\eta - 17) - 6) \right) \right]. \end{aligned}$$

Figure 2 shows that the anisotropy begins at zero in the core and steadily



Table 2: Comparison of  $\rho_{core}$ ,  $P_{r(core)}$  and  $P_{t(core)}$  under different parameter values of  $\zeta$ .

$\zeta$	$\rho_{core}$ ( $10^{27}$ g/cm <sup>3</sup> )	$P_{r(core)}$ ( $10^{36}$ dyn/cm <sup>2</sup> )	$P_{t(core)}$ ( $10^{36}$ dyn/cm <sup>2</sup> )
1.00	8.03	7.03	9.40
1.04	8.57	8.18	9.76
1.08	8.93	9.69	10.18

increases towards the surface of the star. It is well-known that the positive anisotropy indicates stability [54], hence the considered PS is stable.

It is crucial to present numerical values for the physical properties of the PS as predicted by the current model. With  $\zeta = 1.08$ ,  $\rho_{core} \approx 8.93 \times 10^{27}$  g/cm<sup>3</sup>,  $P_{r(core)} \approx 9.69 \times 10^{36}$  dyn/cm<sup>2</sup> and  $P_{t(core)} \approx 10.18 \times 10^{36}$  dyn/cm<sup>2</sup>. At the star's boundary,  $\rho_I$  is  $5.69 \times 10^{27}$  g/cm<sup>3</sup>, which is about 1.8 times the core density. Here  $P_{r(r=R)} = 0$  dyn/cm<sup>2</sup> and  $P_{t(r=R)} \approx 6.12 \times 10^{36}$  dyn/cm<sup>2</sup>. The core values are  $\rho_{core} \approx 8.57 \times 10^{27}$  g/cm<sup>3</sup>,  $P_{r(core)} \approx 8.18 \times 10^{36}$  dyn/cm<sup>2</sup> and  $P_{t(core)} \approx 9.76 \times 10^{36}$  dyn/cm<sup>2</sup> with  $\zeta = 1.04$ . At the star's boundary,  $\rho_I$  is  $5.18 \times 10^{27}$  g/cm<sup>3</sup>, which is about 1.8 times the core density. The radial/tangential pressures are  $P_{r(r=R)} = 0$  dyn/cm<sup>2</sup> and  $P_{t(r=R)} \approx 5.75 \times 10^{36}$  dyn/cm<sup>2</sup>. The core values for  $\zeta = 1$ ,  $\rho_{core} \approx 8.031 \times 10^{27}$  g/cm<sup>3</sup>,  $P_{r(core)} \approx 7.025 \times 10^{36}$  dyn/cm<sup>2</sup> and  $P_{t(core)} \approx 9.40 \times 10^{36}$  dyn/cm<sup>2</sup>. At the star's boundary,  $\rho_I$  is  $4.806 \times 10^{27}$  g/cm<sup>3</sup>, which is about 1.8 times the core density, while  $P_{r(r=R)} = 0$  dyn/cm<sup>2</sup> and  $P_{t(r=R)} \approx 5.51 \times 10^{36}$  dyn/cm<sup>2</sup>. Table 2 provides comparison of  $\rho_{core}$ ,  $P_{r(core)}$  and  $P_{t(core)}$  under different parameter values of  $\zeta$ .

## 4.2 Limit on the Mass-Radius Relation

The mass of the PS is stated as [55]

$$M(r) = 4\pi \int_0^r \chi^2 \rho(\chi) d\chi.$$

The numerical solution of this equation, assessing the reliability of the current model, is shown in Figure 3. The graph clearly demonstrates that the mass increases steadily and uniformly with the star's radius, hence satisfies the physical requirement that mass is always positively increasing function.

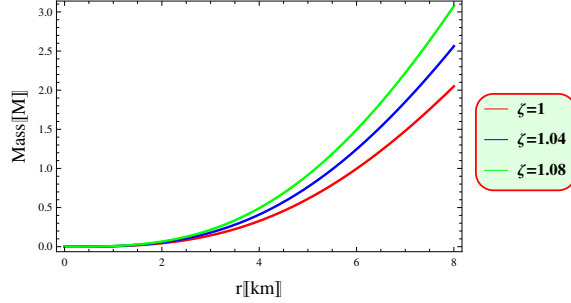


Figure 3: Plot of mass-radius against  $r$ .

### 4.3 The Geometric Component

The gravitational redshift, denoted by  $Z_s(r)$ , describes the change in wavelength (or frequency) of light or other electromagnetic radiation as it escapes from the gravitational field. According to GR, this effect intensifies in stronger gravitational field, particularly around massive objects like stars or black holes. This is defined as follows

$$Z_s(r) = \frac{1}{\sqrt{-g_{tt}}} - 1 = \frac{1}{\sqrt{e^{A_1(\frac{r}{R})^2 + a_1}}} - 1. \quad (40)$$

Utilizing Eq.(33), it can be expressed as

$$Z_s(r) = \frac{1}{\sqrt{1-u}} - 1.$$

We plot  $Z_s(r)$  for the PS considering various values of  $\zeta$ . Ivanov [57] determined that the value of the anisotropic configuration is 5.211. Figure 4 shows that  $Z_s(r)$  remains positive and finite throughout the star's interior, decreasing monotonically [58, 59]. Furthermore, this function stays within the specified limit ( $Z_s < 5.211$ ).

### 4.4 The Zeldovich Condition

The Zeldovich condition is a fundamental criterion in astrophysics that ensures the physical stability of matter under extreme conditions, such as those found in neutron stars and other compact objects. It states that the speed of sound within a material must not exceed the speed of light, ensuring that

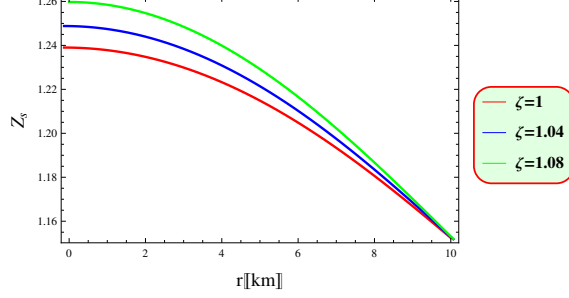


Figure 4: Plot of redshift versus  $r$ .

the EoS remains causal. This condition is derived from relativistic principles, emphasizing that information or perturbations cannot propagate faster than the speed of light. By imposing this restriction, the Zeldovich condition plays a crucial role in determining the viable EoS for dense matter, thereby constraining the physical and theoretical models of cosmic structures. The Zeldovich condition is mathematically expressed as follows

$$\frac{P(0)}{\rho(0)} \leq 1, \quad (41)$$

where  $P(0)$  is the pressure at the center of the star and  $\rho(0)$  is the central density. Let's confirm that this ratio does not exceed 1. The values of  $\rho$ ,  $P_r$  and  $P_t$  as  $r \rightarrow 0$  can be determined as follows

$$\begin{aligned} \rho(0) &= \frac{\zeta(-2a\eta - 17\eta A_1 - 18A_1)}{R^2(-8\eta^2 - 15\eta - 6)}, \\ P_r(0) &= \left[ \frac{\zeta(10a\eta^2 + 26a\eta + 12a - 11\eta^2 A_1 - 13\eta A_1 - 6A_1)}{R^2(1 + \eta)(-8\eta^2 - 15\eta - 6)} \right], \\ P_t(0) &= \frac{\zeta(-14a\eta^2 - 28a\eta - 12a + \eta^2 A_1 + 5\eta A_1 + 6A_1)}{R^2(-8\eta^3 - 23\eta^2 - 21\eta - 6)}. \end{aligned}$$

Utilizing the previously mentioned numerical values for the PS, we can evaluate the Zeldovich inequality (41). From the above expressions, we can find  $\frac{P_r(0)}{\rho(0)} = -0.0842$ , which is less than 1. Similarly, for  $\frac{P_t(0)}{\rho(0)} = 0.3404$ , also less than 1. This confirms the validation of the Zeldovich condition.

## 4.5 Energy Conditions

Astrophysical objects consist of a diverse range of materials and it is crucial to distinguish between the types of matter (ordinary or exotic) that make up these celestial structures. Energy constraints are essential for assessing the possible configurations of fluid matter within such systems. These constraints serve a vital role in understanding specific cosmic structures and the interactions between matter and energy under gravitational forces. For pulsar stars, these constraints ensure the physical feasibility of their internal matter configurations. The energy conditions are classified into four main types.

- Null Energy Condition (NEC): This condition states that the energy density measured along any null vector must be non-negative. Mathematically, it is expressed as

$$0 \leq \rho + P_r, \quad 0 \leq \rho + P_t.$$

This condition does not impose strict relations between matter variables, allowing for scenarios where the pressure may exceed or fall below the energy density.

- Strong Energy Condition: This condition asserts that the sum of three times the energy density and the pressure in any direction must be non-negative. It is defined as

$$0 \leq \rho + P_r, \quad 0 \leq \rho + P_t, \quad 0 \leq \rho + P_r + 2P_t.$$

This condition reflects the combined influence of energy density and pressure in determining matter behavior under gravitational effects.

- Dominant Energy Condition: According to this condition, the energy density must remain non-negative and the corresponding vector field must be time-like or null-like. Mathematically, it is represented as

$$0 \leq \rho \pm P_r, \quad 0 \leq \rho \pm P_t.$$

This condition ensures that energy flows in physically consistent ways across the system.

- **Weak Energy Condition:** This condition requires that the energy density is non-negative as measured by any observer. It is given by

$$0 \leq \rho + P_r, \quad 0 \leq \rho + P_t, \quad 0 \leq \rho.$$

This condition is more stringent than the NEC because it applies to all observers, ensuring the non-negativity of energy density in every frame of reference.

These energy bounds substantially affect the existence of stable astrophysical objects within spacetime. These conditions must be adhered by any feasible cosmic structure. Figure 5 illustrates the energy conditions for different values of  $\zeta$ , represented by the total stress-energy tensor. These plots confirm that the proposed PS satisfies all energy conditions within the context of  $f(\mathcal{Q}, \mathbb{T})$  gravity.

## 4.6 Causality Conditions

The causality condition is a fundamental principle in physics that ensures the relationship between cause and effect remains consistent with the laws of relativity. It states that the speed of sound represents the propagation of signals or disturbances within a medium. This condition preserves the causal structure of spacetime, preventing any violation of relativistic principles where information or influence could travel faster than light. In astrophysics, the causality condition plays a vital role in modeling dense matter, such as in pulsar stars, by constraining equations of state to physically realistic and stable configurations, ensuring that the behavior of matter remains consistent with relativistic causality. The causality condition asserts that the time-like interval between any two events in spacetime must be zero or positive, ensuring that no signal can exceed the speed of light. Based on this, for an anisotropic fluid, this condition results in

$$v_r^2 = \frac{dP_r}{d\rho}, \quad v_t^2 = \frac{dP_t}{d\rho}. \quad (42)$$

In a PS, the squared speed of sound must fall within the range  $[0, 1]$  to maintain structural stability [61]. Both radial and tangential sound speeds meet the stability criteria, with  $0 \leq v_r^2 \leq 1$  and  $0 \leq v_t^2 \leq 1$ . The stability of a PS can be evaluated by examining the cracking condition  $0 \leq |v_t^2 - v_r^2| \leq$

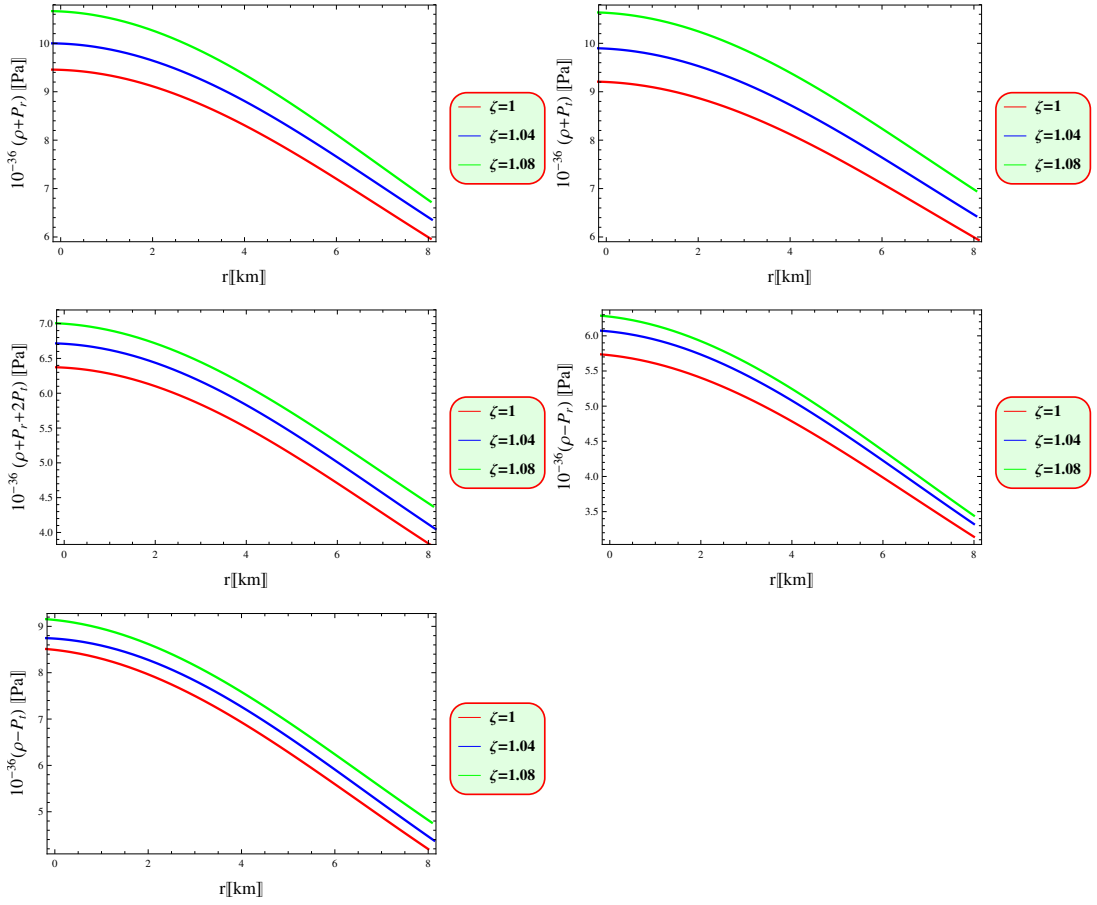


Figure 5: Plots of energy conditions versus  $r$ .

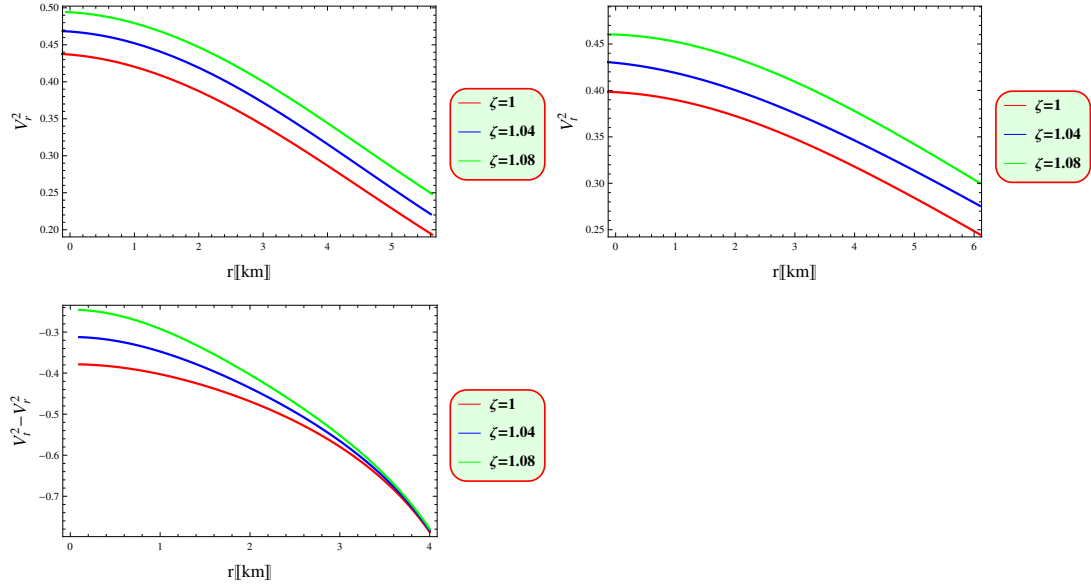


Figure 6: Plots of causality conditions versus  $r$ .

1 [62]. Meeting this criterion indicates that cosmic structures are stable and capable of sustaining their configurations over time. Failure to satisfy this condition suggests instability, potentially leading to the collapse of the structure. This method provides researchers with a valuable tool to assess the stability of cosmic formations, offering critical insights into their behavior and role in the universe. The expressions of the sound speed components are provided in Appendix A. Figure 6 shows the radial and tangential variations of the sound speed with respect to the radial distance. We observe that  $0.44 < v_r^2 < 0.50$  and  $0.40 < v_t^2 < 0.46$ . Additionally, the condition  $-0.79 < v_t^2 - v_r^2 < -0.37$  is maintained throughout the interior of the PS, thereby ensuring stability in its anisotropic stellar configurations.

#### 4.7 The Adiabatic Index and the Equilibrium of Hydrodynamic Forces

To determine the stability of PS, we use the adiabatic index,  $\Gamma$ , defined as [63, 64]

$$\Gamma = \frac{4}{3} \left( \frac{\sigma}{r |\dot{P}_r|} + 1 \right)_{max},$$

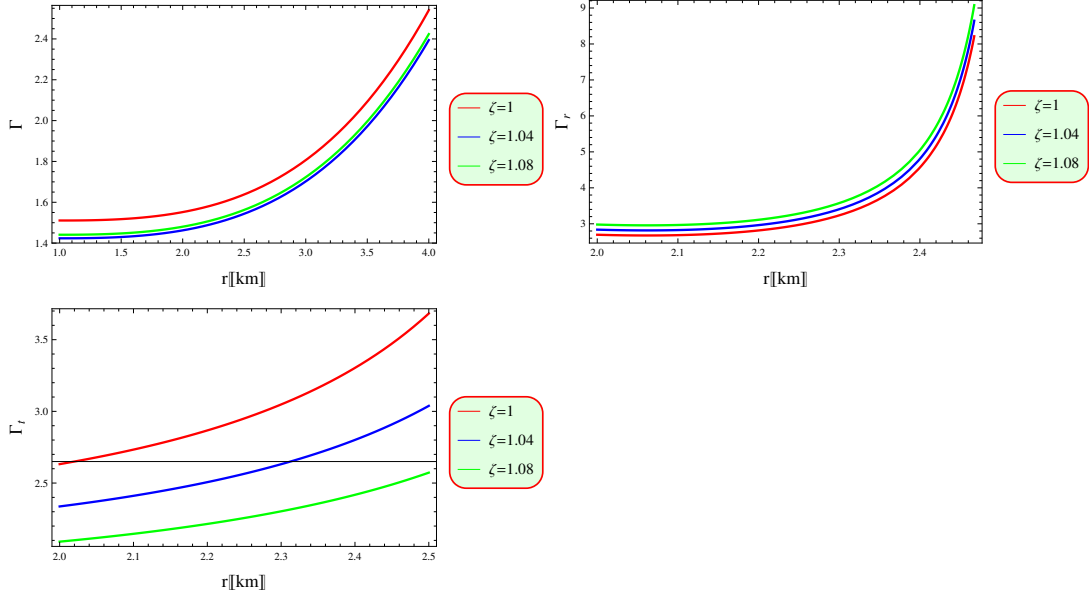


Figure 7: Plots of adiabatic index against  $r$ .

$$\Gamma_r = \frac{\rho + P_r}{P_r} v_r^2, \quad \Gamma_t = \frac{\rho + P_t}{P_t} v_t^2,$$

where the symbols  $\Gamma_r$  and  $\Gamma_t$  represent the radial and tangential components of the adiabatic index, respectively. Clearly, in the case of isotropy ( $\sigma = 0$ ), we get  $\frac{4}{3}$ . For slightly anisotropic condition ( $\sigma \neq 0$ ), similar to those in Newtonian theory,  $\sigma$  is less than  $\frac{4}{3}$ , which is consistent with the usual stability criterion [65]. The adiabatic index can be found in Appendix B. Figure 7 shows a stable anisotropic distribution for the PS across various  $\zeta$  values.

The TOV equation is a key formula in astrophysics that describes the equilibrium of a static spherically symmetric star. It helps to explain how the pressure within a star balances the gravitational forces to maintain stability. It is also essential for understanding the structure and behavior of PS and other compact objects. By solving this equation, scientists can predict the internal pressure, density and overall stability of these dense celestial bodies. The TOV equation for an anisotropic matter distribution is formulated as follows [66]

$$M_G(r) e^{\frac{\alpha-\beta}{2}} \frac{1}{r^2} (\rho + P_r) + \frac{dP_r}{dr} - \frac{2}{r} (P_t - P_r) = 0, \quad (43)$$



where the gravitational mass, denoted as  $M_G$ , is defined as [67, 68]

$$M_G(r) = 4\pi \int (\mathbb{T}_t^t - \mathbb{T}_r^r - \mathbb{T}_\phi^\phi - \mathbb{T}_\theta^\theta) r^2 e^{\frac{\alpha+\beta}{2}} dr. \quad (44)$$

Solving this equation, we obtain

$$M_G(r) = \frac{1}{2} r^2 e^{\frac{\beta-\alpha}{2}} \alpha'. \quad (45)$$

Substituting Eq.(45) into (43), we have

$$\frac{1}{2} \alpha' (\rho + P_r) + \frac{dP_r}{dr} - \frac{2}{r} (P_t - P_r) = 0. \quad (46)$$

We analyze the hydrodynamic equilibrium of our model by utilizing the TOV equation modified for  $f(\mathcal{Q}, \mathbb{T})$  gravity

$$F_a + F_g + F_h + F_{(\mathcal{Q}, \mathbb{T})} = 0, \quad (47)$$

here,  $F_a$ ,  $F_g$  and  $F_h$  denote the anisotropic, gravitational, hydrostatic forces, respectively, along with the force  $F_{(\mathcal{Q}, \mathbb{T})}$ . These forces are described as follows

$$\begin{aligned} F_a &= 2 \frac{\sigma}{r}, & F_g &= \frac{\alpha'(\rho + P_r)}{2}, \\ F_h &= -P'_r, & F_{(\mathcal{Q}, \mathbb{T})} &= P'_r + \frac{\beta'(r)}{2} (\rho - P_r) - \frac{2}{r} (P_t - P_r). \end{aligned}$$

Simplifying the above values, we obtain

$$\begin{aligned} F_a &= \left[ 6\zeta e^{-\frac{A_1 r^2}{R^2}} (a^2 r^4 (8\eta^2 r^2 e^{\frac{A_1 r^2}{R^2}} + \eta (6r^2 e^{\frac{A_1 r^2}{R^2}} - 3) - 2) a r^2 (A_1 r^2 (8\eta^2 r^2 \right. \\ &\quad - e^{\frac{A_1 r^2}{R^2}} + \eta (6r^2 e^{\frac{A_1 r^2}{R^2}} - 3) - 2) + 2R^2 (2(2\eta^2 + 3\eta + 1) r^2 e^{\frac{2A_1 r^2}{R^2}} - (2\eta^2 \\ &\quad + 3\eta + 2(6\eta^2 + 6\eta + 1) r^2 + 1) e^{\frac{A_1 r^2}{R^2}} + 6\eta^2 + 12\eta + 5)) - R^2 (4f\eta^2 r^2 \\ &\quad + 5A_1 \eta r^2 + 2r^2 e^{\frac{2A_1 r^2}{R^2}} (2f(2\eta^2 + 3\eta + 1) r^2 + \eta R^2) - e^{\frac{r^2}{R^2}} (2A_1 r^2 (2\eta^2 \\ &\quad + 3\eta(\eta + 2) r^2 + 1) + R^2 (4\eta^2 + \eta(2r^2 + 5) + 2)) + 4\eta^2 R^2 + 5\eta R^2 \\ &\quad \left. + 2R^2)) \right] \left[ (\eta + 1) r^3 R^4 (8\eta^2 (r^2 e^{\frac{A_1 r^2}{R^2}} - 1) + 3\eta (2r^2 e^{\frac{A_1 r^2}{R^2}} - 5) - 6) \right]^{-1}, \end{aligned}$$

$$\begin{aligned}
F_g = & - \left[ a \zeta e^{-\frac{A_1 r^2}{R^2}} (a^2 \eta (4\eta + 3) r^4 (2r^2 e^{\frac{A_1 r^2}{R^2}} + 1) - a r^2 (R^2 (6(2\eta^2 + 3\eta + 1) \right. \\
& \times r^2 e^{\frac{2A_1 r^2}{R^2}} - (6\eta^2 + 9\eta + (28\eta^2 + 30\eta + 6)r^2 + 3) e^{\frac{A_1 r^2}{R^2}} + 10\eta^2 + 21\eta \\
& + 9) A_1 \eta (4\eta + 3) r^2 (2r^2 e^{\frac{A_1 r^2}{R^2}} + 1)) + R^2 (-A_1 r^2 (6(2\eta^2 + 3\eta + 1) r^2 e^{\frac{2A_1 r^2}{R^2}} \\
& + ((4\eta^2 - 6)r^2 - 3(2\eta^2 + 3\eta + 1)) e^{\frac{A_1 r^2}{R^2}} + 2\eta^2 - 3) - R^2 (e^{\frac{A_1 r^2}{R^2}} - 1) (2\eta^2 \\
& \times (2r^2 e^{\frac{A_1 r^2}{R^2}} - 5) + 3\eta (2r^2 e^{\frac{A_1 r^2}{R^2}} - 5) - 6)) \left. \right] \left[ (\eta + 1) r R^6 (8\eta^2 (r^2 e^{\frac{A_1 r^2}{R^2}} - 1) \right. \\
& + 3\eta (2r^2 e^{\frac{A_1 r^2}{R^2}} - 5) - 6) \left. \right]^{-1},
\end{aligned}$$

$$\begin{aligned}
F_h = & \left[ 2e^{-\frac{A_1 r^2}{R^2}} \zeta (a^2 (A_1 r^2 (16(4e^{\frac{2A_1 r^2}{R^2}} r^4 - 6e^{\frac{A_1 r^2}{R^2}} r^2 + 3)\eta^4 + 2(48e^{\frac{2A_1 r^2}{R^2}} r^4 \right. \\
& - 140e^{\frac{A_1 r^2}{R^2}} r^2 + 97)\eta^3 + 9(4e^{\frac{2A_1 r^2}{R^2}} r^4 - 28e^{\frac{A_1 r^2}{R^2}} r^2 + 31)\eta^2 - 24(3e^{\frac{A_1 r^2}{R^2}} \\
& \times r^2 - 7)\eta + 36) + 36) - R^2 (16(4e^{\frac{2A_1 r^2}{R^2}} r^4 - 8e^{\frac{A_1 r^2}{R^2}} r^2 + 3)\eta^4 \\
& + 2(48e^{\frac{2A_1 r^2}{R^2}} r^4 - 168e^{\frac{A_1 r^2}{R^2}} r^2 + 97)\eta^3 + 3(12e^{\frac{2A_1 r^2}{R^2}} r^4 - 92e^{\frac{A_1 r^2}{R^2}} r^2 + 93)\eta^2 \\
& - 24(3e^{\frac{A_1 r^2}{R^2}} r^2 - 7)\eta + 36)) r^4 - a(4e^{\frac{A_1 r^2}{R^2}} \eta(\eta + 1)(e^{\frac{A_1 r^2}{R^2}} (2\eta^2 + 6\eta + 3) \\
& - 3(2\eta^2 + 3\eta + 1)) R^4 - A_1 (8(-46e^{\frac{A_1 r^2}{R^2}} r^2 + e^{\frac{2A_1 r^2}{R^2}} (26r^2 - 1)r^2 + 21)\eta^4 \\
& + (-980e^{\frac{A_1 r^2}{R^2}} r^2 + 4e^{\frac{2A_1 r^2}{R^2}} (79r^2 - 8)r^2 + 651)\eta^3 + 12(-68e^{\frac{A_1 r^2}{R^2}} r^2 \\
& + e^{\frac{2A_1 r^2}{R^2}} (10r^2 - 3)r^2 + 75)\eta^2 - 6(36e^{\frac{A_1 r^2}{R^2}} r^2 + 2e^{\frac{2A_1 r^2}{R^2}} r^2 - 87)\eta + 108) R^2 \\
& + A_1^2 r^2 (16(4e^{\frac{2A_1 r^2}{R^2}} r^4 - 6e^{\frac{A_1 r^2}{R^2}} r^2 + 3)\eta^4 + 2(48e^{\frac{2A_1 r^2}{R^2}} r^4 - 140e^{\frac{A_1 r^2}{R^2}} r^2 + 97)\eta^3 \\
& + 9(4e^{\frac{2A_1 r^2}{R^2}} r^4 - 28e^{\frac{A_1 r^2}{R^2}} r^2 + 31)\eta^2 - 24(3e^{\frac{A_1 r^2}{R^2}} r^2 - 7)\eta + 36)) r^4 + R^2 \\
& \times (-A_1^2 (8(-2e^{\frac{A_1 r^2}{R^2}} r^2 + e^{\frac{2A_1 r^2}{R^2}} (2r^4 + r^2) + 1)\eta^4 + (-108e^{\frac{A_1 r^2}{R^2}} r^2 \\
& + 4e^{\frac{2A_1 r^2}{R^2}} (11r^2 + 8)r^2 + 63)\eta^3 + 12(-14e^{\frac{A_1 r^2}{R^2}} r^2 + e^{\frac{2A_1 r^2}{R^2}} (2r^2 + 3)r^2 \\
& + 12)\eta^2 + 6(-12e^{\frac{A_1 r^2}{R^2}} r^2 + 2e^{\frac{2A_1 r^2}{R^2}} r^2 + 21)\eta + 36) r^4 - A_1 R^2 \eta (8\eta^3 + 31\eta^2 \\
& + 36\eta - 4e^{\frac{A_1 r^2}{R^2}} r^2 (2\eta^3 + 9\eta^2 + 9\eta + 3) + 4e^{\frac{2A_1 r^2}{R^2}} r^2 (4r^2 \eta^3 3(r^2 + 2)\eta^2 + 9\eta \\
& + 3) + 12)r^2 + (-1 + e^{\frac{A_1 r^2}{R^2}}) R^4 \eta (8(2e^{\frac{2A_1 r^2}{R^2}} r^4 - 2e^{\frac{A_1 r^2}{R^2}} r^2 + 1)\eta^3 + (12
\end{aligned}$$

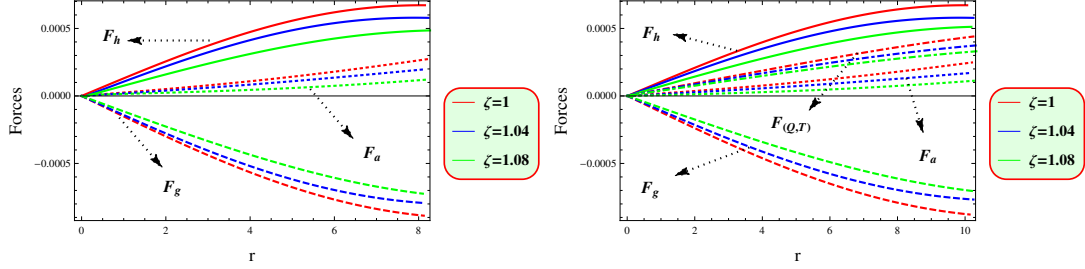


Figure 8: Plots of the TOV equation versus  $r$ .

$$\begin{aligned} & \times \left[ e^{\frac{2A_1 r^2}{R^2}} r^4 - 44e^{\frac{A_1 r^2}{R^2}} r^2 + 31 \right) \eta^2 + (36 - 24e^{\frac{A_1 r^2}{R^2}} r^2) \eta + 12 \Big) \Big] \left[ r^3 R^6 (\eta + 1) \right. \\ & \times \left. \left( 8 \left( e^{\frac{A_1 r^2}{R^2}} r^2 - 1 \right) \eta^2 + 3 \left( 2e^{\frac{A_1 r^2}{R^2}} r^2 - 5 \right) \eta - 6 \right)^2 \right]^{-1}. \end{aligned}$$

Figure 8 shows that our PS remains in equilibrium. This equilibrium is attained because the cumulative effects of  $F_a$ ,  $F_g$ ,  $F_h$ , and  $F_{(Q,T)}$  result in a net sum of zero. This results in a stable model for PS across different values of  $\zeta$ .

## 5 Equation of State Parameter and Compactness

Here, we utilize the following relationships [47]

$$P_r(\rho) \approx v_r^2(\rho - \rho_I), \quad P_t(\rho) \approx v_t^2(\rho - \rho_{II}), \quad (48)$$

where  $\rho_I$  refers to the density at which the radial pressure  $P_r(\rho_I) = 0$ ,  $\rho_I$  and  $\rho_{II}$  denote the densities at the star's surface associated with the radial and tangential pressures, respectively. It is important to note that, unlike  $\rho_I$  which results in  $P_r$  being zero,  $\rho_{II}$  does not necessarily cause  $P_t$  to be zero. The current model fully determines the speed of sound and surface density. For example, when  $\zeta = 1.08$ , using Eqs.(A1) and (A2), we obtain the following values  $v_r^2 \approx 0.49$ ,  $v_t^2 \approx 0.46$ ,  $\rho_I = 5.4 \times 10^{14}$  g/cm<sup>3</sup>, and  $\rho_{II} \approx 4.3 \times 10^{14}$  g/cm<sup>3</sup>. For  $\zeta = 1.04$ ,  $v_r^2 \approx 0.47$ ,  $v_t^2 \approx 0.43$ ,  $\rho_I = 5.6 \times 10^{14}$  g/cm<sup>3</sup>, and  $\rho_{II} \approx 4.2 \times 10^{14}$  g/cm<sup>3</sup>. When  $\zeta = 1$ ,  $v_r^2 \approx 0.44$ ,  $v_t^2 \approx 0.39$ ,  $\rho_I = 5.9 \times 10^{14}$  g/cm<sup>3</sup>, and  $\rho_{II} \approx 4 \times 10^{14}$  g/cm<sup>3</sup>.

The EoS parameter is crucial for characterizing the relationship between  $P$  and  $\rho$  across various physical systems. For a model to be physically viable, the radial and tangential EoS parameters must lie within the range  $[0, 1]$  [69]. This is given as

$$\omega_r = \frac{P_r}{\rho}, \quad \omega_t = \frac{P_t}{\rho}. \quad (49)$$

Inserting Eqs.(37)-(39) into (49), we obtain

$$\begin{aligned} \omega_r = & - \left[ R^4 \left( \frac{1}{R^4} \left\{ 2r^2 \left( -e^{\frac{A_1 r^2}{R^2}} (4a^2 \eta (4\eta + 3) r^4 + a(R^2((\eta + 1)(11\eta + 6) + A_1 R^2 \right. \right. \right. \right. \\ & \times ((\eta + 1)(11\eta + 6) + 2(\eta(27\eta + 29) + 6)r^2) - 4A_1 \eta (4\eta + 3) r^4) + 2(\eta + 2) \\ & \times (\eta + 3) r^2) - 6a^2 \eta^2 r^2 - 4a^2 \eta r^2 + 6af\eta^2 r^2 + 4aA_1 \eta r^2 + 2(\eta + 1)(11\eta + 6) \\ & \times r^2 R^2 (a + A_1) e^{\frac{2A_1 r^2}{R^2}} + 21a\eta^2 R^2 + 43a\eta R^2 + 18aR^2 + 13f\eta^2 R^2 + 21A_1 \eta R^2 \\ & \left. \left. \left. \left. + 6A_1 R^2 \right) \right\} + 2 \left( e^{\frac{A_1 r^2}{R^2}} - 1 \right) (\eta(2(\eta + 3)r^2 e^{\frac{A_1 r^2}{R^2}} - 13\eta - 17) - 6) \right) \right] \left[ 2(\eta + 1) \right. \\ & \times (2a^2 \eta r^4 - 2aA_1 \eta r^4 - 2\eta r^2 R^2 e^{\frac{2A_1 r^2}{R^2}} (r^2(a + A_1) + 3R^2) + R^2 e^{\frac{A_1 r^2}{R^2}} (\eta r^2 (2r^2 \\ & \times (a - 5A_1) + a + A_1) + R^2 (\eta(6r^2 + 7) + 6)) + a\eta r^2 R^2 + 3R^2) + 9A_1 \eta r^2 R^2 \\ & \left. \left. \left. \left. + 12A_1 r^2 R^2 - 7\eta R^4 - 6R^4 \right) \right]^{-1}, \right. \\ \omega_t = & - \left[ (\eta(2(4\eta + 3)r^2 e^{\frac{A_1 r^2}{R^2}} - 8\eta - 15) - 6) (a^2 r^4 (\eta(2(4\eta + 3)r^2 e^{\frac{A_1 r^2}{R^2}} - 6\eta - 13) \right. \\ & - 6) + ar^2 (A_1 r^2 (\eta(-2(4\eta + 3)r^2 e^{\frac{A_1 r^2}{R^2}} + 6\eta + 13) + 6) + R^2 (\eta(e^{\frac{A_1 r^2}{R^2}} (2r^2 \\ & \times (- (\eta + 1) e^{\frac{A_1 r^2}{R^2}} + 9\eta + 7) + \eta + 1) - 15\eta - 29) - 12)) + R^2 (A_1 r^2 (\eta \\ & \times (e^{\frac{A_1 r^2}{R^2}} (-2r^2 ((\eta + 1) e^{\frac{A_1 r^2}{R^2}} + \eta + 2) + \eta + 1) + \eta + 6) + 6) + \eta R^2 (e^{\frac{A_1 r^2}{R^2}} \\ & \left. \left. \left. \left. - 1) (\eta(2r^2 e^{\frac{A_1 r^2}{R^2}} - 1) - 2) \right) \right) \right] \left[ (\eta(2(\eta + 1)(4\eta + 3)r^2 e^{\frac{A_1 r^2}{R^2}} - \eta(8\eta + 23) \right. \right. \\ & - 21) - 6) (2a^2 \eta r^4 - 2aA_1 \eta r^4 - 2\eta r^2 R^2 e^{\frac{2A_1 r^2}{R^2}} (r^2(a + A_1) + 3R^2) + R^2 \\ & \times e^{\frac{A_1 r^2}{R^2}} (\eta r^2 (2r^2(a - 5A_1) + a + A_1) + R^2 (\eta(6r^2 + 7) + 6)) + a\eta r^2 R^2 \\ & \left. \left. \left. \left. + 9A_1 \eta r^2 R^2 + 12A_1 r^2 R^2 - 7\eta R^4 - 6R^4 \right) \right]^{-1}. \right. \end{aligned}$$

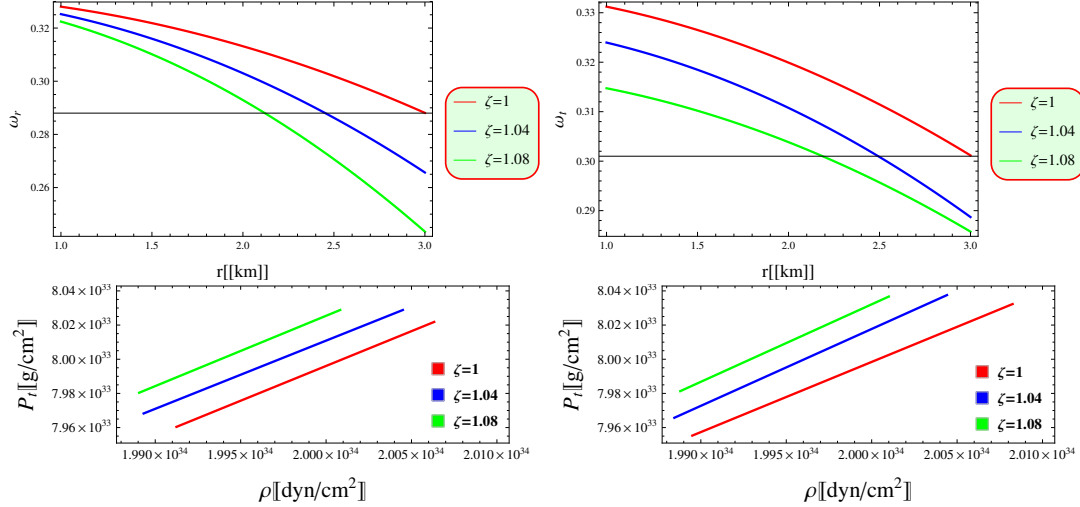


Figure 9: Plots of EoS versus  $r$ .

Figure 9 illustrates the best-fit EoS for the PS, depicting the graphical behavior of density and radial pressure across various values of  $\zeta$ . These results align well with a linear EoS pattern. They also meet the viability criteria for the PS. Similarly, the tangential EoS exhibits a strong correlation with a linear model. The derived EoSs are primarily valid near the star's center and throughout its interior within the range of  $[0, 1]$  [70]. The compactness function  $u = \frac{M(r)}{r}$  is essential in assessing the viability of a PS. Buchdahl [71] proposed a limit for the mass-radius ratio, stating that  $u$  must be less than  $\frac{4}{9}$  for a PS to be viable. Figure 10 demonstrates that compactness increases steadily remaining within the specified limit of ( $u < \frac{4}{9}$ ).

## 6 Concluding Remarks

In this paper, we have explored PS in the framework of  $f(\mathcal{Q}, \mathbb{T})$  theory of gravity for a particular model  $f(\mathcal{Q}, \mathbb{T}) = \zeta \mathcal{Q} + \eta \mathbb{T}$ . We have explored how this theory changes our understanding of PS and found that these modifications significantly affect its composition and dynamics. Focusing on an anisotropic fluid scenario and assuming the KB ansatz for the star's inner region, we have identified crucial limits on our model parameters. The key results are summarized as follows.

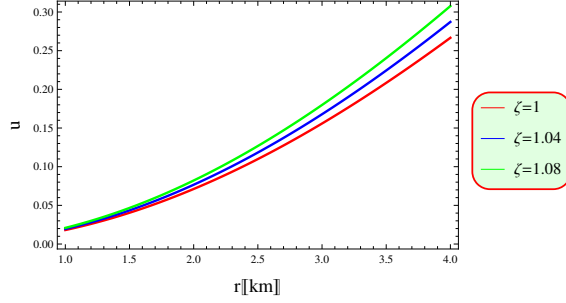


Figure 10: Plot of compactness versus  $r$ .

- We have shown that  $\rho$ ,  $P_r$  and  $P_t$  for various values of  $\zeta$  are highest at the center and decrease towards the surface. The radial pressure  $P_r$  reaches zero at the surface of the star (Figure 1).
- The anisotropy is zero at the center where  $P_t = P_r$  but becomes positive in other regions (Figure 2). This behavior indicates that the model aligns with theoretical predictions and validates the physical viability of the proposed stellar structure.
- The mass function for the PS clearly demonstrates that the mass of the star steadily and uniformly increases with the radius (Figure 3). This observation aligns with the stability of the PS.
- The redshift function decreases monotonically and remains within the  $Z_s < 5.211$  limit (Figure 4). This is consistent with theoretical expectations.
- The energy conditions for various values of  $\zeta$  confirm that the proposed PS meets all energy conditions, validating the physical viability of our model (Figure 5).
- We have observed that the sound speed propagates in both radial and tangential directions for PS at various values of  $\zeta$  (Figure 6). Furthermore, we have found that  $(-1 < |v_t^2 - v_r^2| < 0)$  throughout the pulsar's interior, ensuring stability in its anisotropic stellar configurations.
- The condition  $\Gamma > \frac{4}{3}$  is satisfied (Figure 7), validating the physical stability of PS for various values of  $\zeta$ .

- We have determined that equilibrium is achieved as the sum of the combined forces  $F_a$ ,  $F_g$ ,  $F_h$  and  $F_{(\mathcal{Q}, \mathbb{T})}$  equals to zero (Figure 8). This leads to a stable model for the PS across various values of  $\zeta$ .
- The EoS for the PS demonstrates a strong linear relationship between density and radial pressure for all values of  $\zeta$ . The tangential pressure also fits well with a linear model. These equations hold true near the center and throughout the interior of the star within the range of 0 to 1. This confirms that  $\omega_r$  and  $\omega_t$  meet the criteria for PS viability, suggesting enhanced stability (Figure 9).
- The compactness gradually increases throughout the star's interior and remains within the specified limits of  $u < \frac{4}{9}$  for various values of  $\zeta$  (Figure 10).

Our results indicate that  $f(\mathcal{Q}, \mathbb{T})$  gravity offers a new and fascinating perspective for understanding PS. It is worth noting that this theory satisfies both the stability criteria and empirical observations. Moreover, our findings align with the recent literature [47] that support the viability of  $f(\mathcal{Q}, \mathbb{T})$  gravity in explaining the complexities of astrophysical phenomena. The continued exploration and advancement in this domain hold significant potential for enhancing our understanding of the universe. Future research in this area promises to refine and rigorously test these models, potentially revealing the new insights into the fundamental nature of gravity and the dynamics of compact objects like PS.

Despite these advancements, the application of  $f(\mathcal{Q}, \mathbb{T})$  gravity to strong-field regimes, particularly compact astrophysical objects like neutron stars and pulsars, remains under explored. Compact stars, formed during supernova collapses, exhibit extreme gravitational and matter densities, making them ideal laboratories for testing modifications to GR. The PS, with its observed mass and radius properties, provides a compelling case for exploring these theories in anisotropic stellar configurations. Through our analysis, we have demonstrated that the PS within the  $f(\mathcal{Q}, \mathbb{T})$  modified gravity framework exhibits a dense and stable profile. Key physical quantities, including density, pressure and anisotropy, show extended ranges that make this star physically viable and stable, even at its center. This marks a significant improvement over predictions from GR and other modified gravity theories, where compact stars often fail to maintain stability in central regions. To validate our findings, we have analyzed critical parameters such as energy con-

ditions, compactness, redshift and the adiabatic index, which further confirm the dense and stable nature of the PS within this framework. By systematically exploring the impact of  $f(\mathcal{Q}, \mathbb{T})$  gravity, this study addresses existing gaps in the literature and advances our understanding of strong-field astrophysics, offering a more viable and comprehensive description of anisotropic stellar structures.

The  $f(\mathcal{Q}, \mathbb{T})$  gravity is a powerful extension of GR. This theory broadens GR applicability to regions with strong gravitational fields where GR often struggles. One major strength of this theory is its ability to model anisotropic stellar configurations, making it particularly suitable for compact objects such as pulsars. In this study, stable configurations have been successfully predicted for PS, satisfying essential physical criteria like the mass-radius relation, redshift, causality conditions and the Zeldovich condition. Furthermore, the theory aligns well with observational data, providing a robust framework for describing compact stellar structures while accommodating complex matter distributions. By directly linking geometry with matter,  $f(\mathcal{Q}, \mathbb{T})$  gravity unifies gravitational and matter interactions in a way that GR cannot achieve in strong-field regimes.

Despite its strengths,  $f(\mathcal{Q}, \mathbb{T})$  gravity has certain limitations that require further investigation. The theory's predictions depend on the parameters  $\zeta$  and  $\eta$ , which govern the functional form of the theory. These parameters currently lack direct observational constraints and aligning theoretical results with astrophysical data necessitates fine adjustments. This sensitivity reduces the universality of the theory and limits its predictive power. Moreover, the mathematical complexity of the field equations poses another challenge, as deriving analytical solutions is often difficult, leading to a reliance on numerical methods. Such reliance on numerical approximations can introduce uncertainties, particularly when modeling precise astrophysical phenomena. Additionally, while this study has demonstrated the theory applicability to a single pulsar, its application to a broader range of compact objects and cosmological phenomena remains to be tested.

In summary,  $f(\mathcal{Q}, \mathbb{T})$  gravity is a significant and robust theoretical framework designed to explain compact stars and observational data, particularly in strong-field gravitational environments. Its ability to unify geometry and matter interactions makes it a promising extension of GR. However, its dependence on tunable parameters and the complexity of its equations highlight the need for further research. By pursuing applications in astrophysics, gravitational wave science and cosmology, and refining its mathematical frame-



work,  $f(\mathcal{Q}, \mathbb{T})$  gravity has the potential to play a pivotal role in advancing our understanding of the universe.

## Appendix A: Casuality Condition

The expressions of squared sound speed in the radial and tangential directions are given as follows.

$$\begin{aligned}
v_r^2 = & \left[ (\eta + 1) \left( A_1^2 \left( 2a\eta \left( 8 \left( 2e^{\frac{A_1 r^2}{R^2}} r^2 - 1 \right) \eta^2 + 3 \left( 4e^{\frac{A_1 r^2}{R^2}} r^2 - 5 \right) \eta - 6 \right) r^2 \right. \right. \right. \\
& + R^2 \left( 8 \left( -18e^{\frac{A_1 r^2}{R^2}} r^2 + e^{\frac{2A_1 r^2}{R^2}} (10r^4 + r^2) + 9 \right) \eta^3 + 3 \left( -100e^{\frac{A_1 r^2}{R^2}} r^2 + 4 \right. \right. \\
& \times e^{\frac{2A_1 r^2}{R^2}} (5r^2 + 2) r^2 + 77) \eta^2 + 6 \left( -24e^{\frac{A_1 r^2}{R^2}} r^2 + 2e^{\frac{2A_1 r^2}{R^2}} r^2 + 39 \right) \eta \\
& + 72) \Big) r^4 + A_1 \left( -2a^2 \eta \left( 8 \left( 2e^{\frac{A_1 r^2}{R^2}} r^2 - 1 \right) \eta^2 + 3 \left( 4e^{\frac{A_1 r^2}{R^2}} r^2 - 5 \right) \eta - 6 \right) r^4 \right. \\
& - aR^2 \eta \left( 4e^{\frac{A_1 r^2}{R^2}} \eta (4\eta + 3) r^2 + 4e^{\frac{2A_1 r^2}{R^2}} ((4r^2 - 2)\eta^2 + 3(r^2 - 2)\eta - 3) r^2 \right. \\
& - 3(8\eta^2 + 15\eta + 6)) r^2 + R^4 \left( -8 \left( 6e^{\frac{2A_1 r^2}{R^2}} r^4 - 15e^{\frac{A_1 r^2}{R^2}} r^2 + 7 \right) \eta^3 \right. \\
& - 3 \left( -60e^{\frac{a r^2}{R^2}} r^2 + 4e^{\frac{2A_1 r^2}{R^2}} (3r^2 - 2) r^2 + 51 \right) \eta^2 + 12 \left( 5e^{\frac{A_1 r^2}{R^2}} r^2 + e^{\frac{2A_1 r^2}{R^2}} r^2 \right. \\
& - 11) \eta - 36) \Big) r^2 + R^2 \left( -2a^2 \eta (8\eta^2 + 15\eta + 6) r^4 + 4ae^{\frac{A_1 r^2}{R^2}} R^2 \eta \left( e^{\frac{A_1 r^2}{R^2}} \right. \right. \\
& \times (2\eta^2 + 6\eta + 3) - 3(2\eta^2 + 3\eta + 1)) r^4 + \left( -1 + e^{\frac{A_1 r^2}{R^2}} \right) R^4 \left( 8 \left( 6e^{\frac{2A_1 r^2}{R^2}} r^4 \right. \right. \\
& - 14e^{\frac{A_1 r^2}{R^2}} r^2 + 7) \eta^3 + 9 \left( 4e^{\frac{2A_1 r^2}{R^2}} r^4 - 20e^{\frac{A_1 r^2}{R^2}} r^2 + 17 \right) \eta^2 + (132 - 72e^{\frac{A_1 r^2}{R^2}} r^2) \eta \\
& + 36) \Big) \Big] \left[ -2a^2 \eta (A_1 r^2 (8(8e^{\frac{2A_1 r^2}{R^2}} r^4 + 6e^{\frac{A_1 r^2}{R^2}} r^2 - 3) \eta^3 + (96e^{\frac{2A_1 r^2}{R^2}} r^4 + 68 \right. \right. \\
& \times e^{\frac{A_1 r^2}{R^2}} r^2 - 61) \eta^2 + 12(3e^{\frac{2A_1 r^2}{R^2}} r^4 + 2e^{\frac{A_1 r^2}{R^2}} r^2 - 4) \eta - 12) - R^2 (4e^{\frac{2A_1 r^2}{R^2}} \eta \\
& \times (4\eta + 3)^2 r^4 - 4e^{\frac{A_1 r^2}{R^2}} (32\eta^3 + 84\eta^2 + 69\eta + 18) r^2 - 24\eta^3 - 61\eta^2 - 48\eta \\
& - 12) \Big) r^4 + a \left( 4e^{\frac{A_1 r^2}{R^2}} (11\eta^2 + 17\eta + 6) \left( e^{\frac{A_1 r^2}{R^2}} (2\eta^2 + 6\eta + 3) - 3(2\eta^2) \right) \right. \\
& \times R^4 - A_1 \left( -4e^{\frac{A_1 r^2}{R^2}} \eta (148\eta^3 + 403\eta^2 + 339\eta + 90) r^2 + 4e^{\frac{2A_1 r^2}{R^2}} (2(70r^2 \right. \\
& - 11) \eta^4 + 5(49r^2 - 20) \eta^3 + 3(43r^2 - 49) \eta^2 + 3(6r^2 - 29) \eta - 18) r^2 \\
& + 3(40\eta^4 + 179\eta^3 + 273\eta^2 + 168\eta + 36) \Big) R^2 + 2A_1^2 r^2 \eta \left( 8 \left( 8e^{\frac{2A_1 r^2}{R^2}} r^4 \right. \right.
\end{aligned}$$

$$\begin{aligned}
& + 6e \frac{A_1 r^2}{R^2} r^2 - 3) \eta^3 + (96e \frac{2A_1 r^2}{R^2} r^4 + 68e \frac{A_1 r^2}{R^2} r^2 - 61) \eta^2 + 12(3e \frac{2A_1 r^2}{R^2} r^4 \\
& + 2e \frac{A_1 r^2}{R^2} r^2 - 4) \eta - 12)) r^4 + R^2 (-A_1^2 (104\eta^4 + 363\eta^3 + 441\eta^2 - 4e \frac{A_1 r^2}{R^2} r^2 \\
& \times (52\eta^3 + 123\eta^2 + 87\eta + 18) \eta + 216\eta + 4e \frac{2A_1 r^2}{R^2} r^2 ((4r^2 - 22)\eta^4 + (23r^2 \\
& - 100)\eta^3 + 3(13r^2 - 49)\eta^2 + 3(6r^2 - 29)\eta - 18) + 36)r^4 - A_1 R^2 (104\eta^4 \\
& + 331\eta^3 + 381\eta^2 + 192\eta - 4e \frac{A_1 r^2}{R^2} r^2 (74\eta^4 + 141\eta^3 + 54\eta^2 - 33\eta - 18) \\
& + 4e \frac{2A_1 r^2}{R^2} r^2 (4r^2 \eta^4 + 3(5r^2 - 22)\eta^3 + 9(r^2 - 15)\eta^2 - 87\eta - 18) + 36)r^2 \\
& + (-1 + e \frac{A_1 r^2}{R^2}) R^4 (8(2e \frac{2A_1 r^2}{R^2} r^4 - 26e \frac{A_1 r^2}{R^2} r^2 + 13)\eta^4 + (60e \frac{2A_1 r^2}{R^2} r^4 - 428 \\
& \times e \frac{A_1 r^2}{R^2} r^2 + )^3 + (e \frac{2r^2}{R^2} r^4 - e \frac{A_1 r^2}{R^2} r^2 + ) \eta^2 - (e \frac{A_1 r^2}{R^2} r^2 - 8)\eta + )) \Big]^{-1}, \quad (A1)
\end{aligned}$$

$$\begin{aligned}
v_t^2 = & \left[ (\eta + 1) (A_1^2 (2a\eta (8(2e \frac{A_1 r^2}{R^2} r^2 - 1)\eta^2 + 3(4e \frac{A_1 r^2}{R^2} r^2 - 5)\eta - 6)r^2 + R^2 (8 \right. \\
& \times e \frac{A_1 r^2}{R^2} r^2 + e \frac{2A_1 r^2}{R^2} (10r^4 + r^2) + 9)\eta^3 + 3(-100e \frac{A_1 r^2}{R^2} r^2 + 4e \frac{2A_1 r^2}{R^2} (5r^2 + 2)r^2 \\
& + 6(-24e \frac{A_1 r^2}{R^2} r^2 + 2e \frac{2A_1 r^2}{R^2} r^2 + 39)\eta + 72))r^4 + A_1 (-2a^2\eta (8(2e \frac{A_1 r^2}{R^2} r^2 - 1)\eta^2 \\
& + 3(4e \frac{A_1 r^2}{R^2} r^2 - 5)\eta - 6)r^4 - aR^2\eta (4e \frac{A_1 r^2}{R^2} \eta (4\eta + 3)r^2 + 4e \frac{2A_1 r^2}{R^2} ((4r^2 - 2) \\
& \times \eta^2 + 3(r^2 - 2)\eta - 3)r^2 - 3(8\eta^2 + 15\eta + 6))r^2 + R^4 (-8(6e \frac{2A_1 r^2}{R^2} r^4 \\
& - 15e \frac{A_1 r^2}{R^2} r^2 + 7)\eta^3 - 3(-60e \frac{A_1 r^2}{R^2} r^2 + 4e \frac{2A_1 r^2}{R^2} (3r^2 - 2)r^2 + 51)\eta^2 + 12 \\
& \times (5e \frac{A_1 r^2}{R^2} r^2 + e \frac{2A_1 r^2}{R^2} r^2 - 11)\eta - 36))r^2 + R^2 (-2a^2\eta (8\eta^2 + 15\eta + 6)r^4 \\
& + 4ae \frac{A_1 r^2}{R^2} R^2\eta (e \frac{A_1 r^2}{R^2} (2\eta^2 + 6\eta + 3) - 3(2\eta^2 + 3\eta + 1))r^4 + (-1 + e \frac{A_1 r^2}{R^2}) \\
& \times R^4 (8(6e \frac{2A_1 r^2}{R^2} r^4 - 14e \frac{A_1 r^2}{R^2} r^2 + 7)\eta^3 + 9(4e \frac{2A_1 r^2}{R^2} r^4 - 20e \frac{A_1 r^2}{R^2} r^2 + 17)\eta^2 \\
& + (132 - 72e \frac{A_1 r^2}{R^2} r^2)\eta + 36)) \Big] \left[ a^2 (A_1 r^2 (16(4e \frac{2A_1 r^2}{R^2} r^4 - 6e \frac{A_1 r^2}{R^2} r^2 + 3)\eta^4 \right. \\
& + 2(48e \frac{2A_1 r^2}{R^2} r^4 - 140e \frac{A_1 r^2}{R^2} r^2 + 97)\eta^3 + 9(4e \frac{2A_1 r^2}{R^2} r^4 - 28e \frac{A_1 r^2}{R^2} r^2 + 31)\eta^2 \\
& - 24(3e \frac{A_1 r^2}{R^2} r^2 - 7)\eta + 36) - R^2 (16(4e \frac{2A_1 r^2}{R^2} r^4 - 8e \frac{A_1 r^2}{R^2} r^2 + 3)\eta^4 + 2 \\
& \times (48e \frac{2A_1 r^2}{R^2} r^4 - 168e \frac{A_1 r^2}{R^2} r^2 + 97)\eta^3 + 3(12e \frac{2f r^2}{R^2} r^4 - 92e \frac{A_1 r^2}{R^2} r^2 + 93)\eta^2
\end{aligned}$$

$$\begin{aligned}
& - 24(3e^{\frac{A_1 r^2}{R^2}} r^2 - 7)\eta + 36))r^4 - a(4e^{\frac{A_1 r^2}{R^2}} \eta(\eta + 1)(e^{\frac{A_1 r^2}{R^2}} (2\eta^2 + 6\eta + 3) \\
& - (2\eta^2 + 3\eta + 1))R^4 - A_1(8(-46e^{\frac{A_1 r^2}{R^2}} r^2 + e^{\frac{2A_1 r^2}{R^2}} (26r^2 - 1)r^2 + 21)\eta^4 \\
& + (-980e^{\frac{A_1 r^2}{R^2}} r^2 + 4e^{\frac{2A_1 r^2}{R^2}} (79r^2 - 8)r^2 + 651)\eta^3 + 12(-68e^{\frac{A_1 r^2}{R^2}} r^2 \\
& + e^{\frac{2A_1 r^2}{R^2}} (10r^2 - 3)r^2 + 75)\eta^2 - 6(36e^{\frac{A_1 r^2}{R^2}} r^2 + 2e^{\frac{2A_1 r^2}{R^2}} r^2 - 87)\eta + 108)R^2 \\
& + A_1^2 r^2 (16(4e^{\frac{2A_1 r^2}{R^2}} r^4 - 6e^{\frac{A_1 r^2}{R^2}} r^2 + 3)\eta^4 + 2(48e^{\frac{2A_1 r^2}{R^2}} r^4 - 140e^{\frac{A_1 r^2}{R^2}} r^2 + 97)\eta^3 \\
& + 9(4e^{\frac{2A_1 r^2}{R^2}} r^4 - 28e^{\frac{A_1 r^2}{R^2}} r^2 + 31)\eta^2 - 24(3e^{\frac{A_1 r^2}{R^2}} r^2 - 7)\eta + 36))r^4 \\
& + R^2(-A_1^2(8(-2e^{\frac{A_1 r^2}{R^2}} r^2 + e^{\frac{2A_1 r^2}{R^2}} (2r^4 + r^2) + 1)\eta^4 + (-108e^{\frac{A_1 r^2}{R^2}} r^2 + 4 \\
& \times e^{\frac{2A_1 r^2}{R^2}} (11r^2 + 8)r^2 + 63)\eta^3 + 12(-14e^{\frac{A_1 r^2}{R^2}} r^2 + e^{\frac{2A_1 r^2}{R^2}} (2r^2 + 3)r^2 + 12)\eta^2 \\
& + 6(-12e^{\frac{A_1 r^2}{R^2}} r^2 + 2e^{\frac{2A_1 r^2}{R^2}} r^2 + 21)\eta + 36)r^4 - A_1 R^2 \eta (8\eta^3 + 31\eta^2 + 36\eta - 4 \\
& \times e^{\frac{A_1 r^2}{R^2}} r^2 (2\eta^3 + 9\eta^2 + 9\eta + 3) + 4e^{\frac{2A_1 r^2}{R^2}} r^2 (4r^2 \eta^3 + 3(r^2 + 2)\eta^2 + 9\eta + 3) \\
& + 12)r^2 + (-1 + e^{\frac{A_1 r^2}{R^2}})R^4 \eta (8(2e^{\frac{2A_1 r^2}{R^2}} r^4 - 2e^{\frac{A_1 r^2}{R^2}} r^2 + 1)\eta^3 + (12e^{\frac{2A_1 r^2}{R^2}} r^4 \\
& - 44e^{\frac{A_1 r^2}{R^2}} r^2 + 31)\eta^2 + (36 - 24e^{\frac{A_1 r^2}{R^2}} r^2)\eta + 12)) \Big]^{-1}. \tag{A2}
\end{aligned}$$

## Appendix B: Adiabatic Index

The expressions of the adiabatic index is given as follows.

$$\begin{aligned}
\Gamma &= \frac{4}{3} \left[ 1 - \left\{ 3R^2(8(e^{\frac{A_1 r^2}{R^2}} r^2 - 1)\eta^2 + 3(2e^{\frac{A_1 r^2}{R^2}} r^2 - 5)\eta - 6)(-a^2(8e^{\frac{A_1 r^2}{R^2}} r^2 \eta^2 \right. \right. \\
& + (6e^{\frac{A_1 r^2}{R^2}} r^2 - 3)\eta - 2)r^4 + a(A_1(8e^{\frac{A_1 r^2}{R^2}} r^2 \eta^2 + (6e^{\frac{A_1 r^2}{R^2}} r^2 - 3)\eta - 2)r^2 + 2R^2 \\
& \times (2e^{\frac{2A_1 r^2}{R^2}} (2\eta^2 + 3\eta + 1)r^2 + 6\eta^2 + 12\eta - e^{\frac{A_1 r^2}{R^2}} (2(6\eta^2 + 6\eta + 1)r^2 + 2\eta^2 \\
& + 3\eta + 1) + 5))r^2 + R^2(4a\eta^2 r^2 + 5A_1 \eta r^2 + 2e^{\frac{2A_1 r^2}{R^2}} (2A_1(2\eta^2 + 3\eta + 1)r^2 \\
& + R^2 \eta)r^2 + 2R^2 + 4R^2 \eta^2 + 5R^2 \eta - e^{\frac{A_1 r^2}{R^2}} (2A_1((\eta + 2)r^2 + 2\eta^2 + 3\eta + 1)r^2 \\
& + R^2(4\eta^2 + (2r^2 + 5)\eta + 2)))) \Big\} \Big\{ 2(2a^2 \eta (a r^2 (8(8e^{\frac{2A_1 r^2}{R^2}} r^4 + 6e^{\frac{A_1 r^2}{R^2}} r^2 - 3)\eta^3
\end{aligned}$$

$$\begin{aligned}
& + \left( 96e^{\frac{2A_1r^2}{R^2}}r^4 + 68e^{\frac{A_1r^2}{R^2}}r^2 - 61 \right) \eta^2 + 12 \left( 3e^{\frac{2A_1r^2}{R^2}}r^4 + 2e^{\frac{A_1r^2}{R^2}}r^2 - 4 \right) \eta - 12 \\
& - R^2 \left( 4e^{\frac{2A_1r^2}{R^2}}\eta(4\eta + 3)^2r^4 - 4e^{\frac{A_1r^2}{R^2}}(32\eta^3 + 84\eta^2 + 69\eta + 18)r^2 - 24\eta^3 \right. \\
& - 61\eta^2 - 48\eta - 12) \left. \right) r^4 - a \left( 4e^{\frac{A_1r^2}{R^2}}(11\eta^2 + 17\eta + 6) \left( e^{\frac{A_1r^2}{R^2}}(2\eta^2 + 6\eta + 3) \right. \right. \\
& - 3(2\eta^2 + 3\eta + 1)) R^4 - A_1 \left( -4e^{\frac{A_1r^2}{R^2}}\eta(148\eta^3 + 403\eta^2 + 339\eta + 90)r^2 \right. \\
& + 4e^{\frac{2A_1r^2}{R^2}}(2(70r^2 - 11)\eta^4 + 5(49r^2 - 20)\eta^3 + 3(43r^2 - 49)\eta^2 \\
& + 3(6r^2 - 29)\eta - 18)r^2 + 3(40\eta^4 + 179\eta^3 + 273\eta^2 + 168\eta + 36)) R^2 \\
& + 2A_1^2r^2\eta(8(8e^{\frac{2A_1r^2}{R^2}}r^4 + 6e^{\frac{A_1r^2}{R^2}}r^2 - 3)\eta^3 + (96e^{\frac{2A_1r^2}{R^2}}r^4 + 68e^{\frac{A_1r^2}{R^2}}r^2 - 61)\eta^2 \\
& + 12(3e^{\frac{2A_1r^2}{R^2}}r^4 + 2e^{\frac{A_1r^2}{R^2}}r^2 - 4)\eta - 12))r^4 + R^2(A_1^2(104\eta^4 + 363\eta^3 + 441\eta^2 \\
& - 4e^{\frac{A_1r^2}{R^2}}r^2(52\eta^3 + 123\eta^2 + 87\eta + 18)\eta + 216\eta + 4e^{\frac{2A_1r^2}{R^2}}r^2((4r^2 - 22)\eta^4 \\
& + (23r^2 - 100)\eta^3 + 3(13r^2 - 49)\eta^2 + 3(6r^2 - 29)\eta - 18) + 36)r^4 \\
& + aR^2(104\eta^4 + 331\eta^3 + 381\eta^2 + 192\eta - 4e^{\frac{A_1r^2}{R^2}}r^2(74\eta^4 + 141\eta^3 + 54\eta^2 \\
& - 33\eta - 18) + 4e^{\frac{2A_1r^2}{R^2}}r^2(4r^2\eta^4 + 3(5r^2 - 22)\eta^3 + 9(r^2 - 15)\eta^2 - 87\eta - 18) \\
& + 36)r^2 - (-1 + e^{\frac{A_1r^2}{R^2}})R^4(8(2e^{\frac{2A_1r^2}{R^2}}r^4 - 26e^{\frac{A_1r^2}{R^2}}r^2 + 13)\eta^4 + (60e^{\frac{2A_1r^2}{R^2}}r^4 \\
& - 428e^{\frac{A_1r^2}{R^2}}r^2 + 331)\eta^3 + (36e^{\frac{2A_1r^2}{R^2}}r^4 - 300e^{\frac{A_1r^2}{R^2}}r^2 + 381)\eta^2 \\
& - 24(3e^{\frac{A_1r^2}{R^2}}r^2 - 8)\eta + 36)) \left. \right\}^{-1} \Big],
\end{aligned}$$

$$\begin{aligned}
\Gamma_r = & \left[ 4(\eta + 1) \left( \eta \left( 2e^{\frac{A_1r^2}{R^2}}(4\eta + 3)r^2 - 8\eta - 15 \right) - 6 \right) \left( A_1^2(2a\eta(8(2e^{\frac{A_1r^2}{R^2}}r^2 \right. \right. \right. \\
& - 1)\eta^2 + 3(4e^{\frac{A_1r^2}{R^2}}r^2 - 5)\eta - 6)r^2 + R^2(8(-18e^{\frac{A_1r^2}{R^2}}r^2 + e^{\frac{2A_1r^2}{R^2}}(10r^4 + r^2) \\
& + 9)\eta^3 + 3(-100e^{\frac{A_1r^2}{R^2}}r^2 + 4e^{\frac{2A_1r^2}{R^2}}(5r^2 + 2)r^2 + 77)\eta^2 + 6(-24e^{\frac{A_1r^2}{R^2}}r^2 \\
& + 2e^{\frac{2A_1r^2}{R^2}}r^2 + 39)\eta + 72))r^4 + a(-2a^2\eta(8(2e^{\frac{A_1r^2}{R^2}}r^2 - 1)\eta^2 + 3(4e^{\frac{A_1r^2}{R^2}}r^2 \\
& - 5)\eta - 6)r^4 - aR^2\eta(4e^{\frac{A_1r^2}{R^2}}\eta(4\eta + 3)r^2 + 4e^{\frac{2A_1r^2}{R^2}}((4r^2 - 2)\eta^2 + 3(r^2 \\
& - 2)\eta - 3)r^2 - 3(8\eta^2 + 15\eta + 6))r^2 + R^4(-8(6e^{\frac{2A_1r^2}{R^2}}r^4 - 15e^{\frac{A_1r^2}{R^2}}r^2 \\
& + 7)\eta^3 - 3(-60e^{\frac{A_1r^2}{R^2}}r^2 + 4e^{\frac{2A_1r^2}{R^2}}(3r^2 - 2)r^2 + 51)\eta^2 + 12(5e^{\frac{A_1r^2}{R^2}}r^2
\end{aligned}$$

$$\begin{aligned}
& + e^{\frac{2A_1 r^2}{R^2}} r^2 - 11) \eta - 36)) r^2 + R^2 (-2a^2 \eta (8\eta^2 + 15\eta + 6) r^4 + 4ae^{\frac{f r^2}{R^2}} \\
& \times R^2 \eta (e^{\frac{A_1 r^2}{R^2}} (2\eta^2 + 6\eta + 3) - 3(2\eta^2 + 3\eta + 1)) r^4 + (-1 + e^{\frac{A_1 r^2}{R^2}}) \\
& \times R^4 (8(6e^{\frac{2A_1 r^2}{R^2}} r^4 - 14e^{\frac{A_1 r^2}{R^2}} r^2 + 7) \eta^3 + 9(4e^{\frac{2A_1 r^2}{R^2}} r^4 - 20e^{\frac{A_1 r^2}{R^2}} r^2 + 17) \eta^2 \\
& + (132 - 72e^{\frac{A_1 r^2}{R^2}} r^2) \eta + 36))) (-a^2 (2e^{\frac{A_1 r^2}{R^2}} r^2 + 1) \eta (4\eta + 3) r^4 \\
& + a(A_1 (2e^{\frac{A_1 r^2}{R^2}} r^2 + 1) \eta (4\eta + 3) r^2 + R^2 (6e^{\frac{2A_1 r^2}{R^2}} (2\eta^2 + 3\eta + 1) r^2 \\
& + 10\eta^2 + 21\eta - e^{\frac{A_1 r^2}{R^2}} ((28\eta^2 + 30\eta + 6) r^2 + 6\eta^2 + 9\eta + 3) + 9)) r^2 \\
& + R^2 (a(6e^{\frac{2A_1 r^2}{R^2}} (2\eta^2 + 3\eta + 1) r^2 + 2\eta^2 + e^{\frac{A_1 r^2}{R^2}} (r^2 (4\eta^2 - 6) - 3(2\eta^2 \\
& + 3\eta + 1)) - 3) r^2 + (-1 + e^{\frac{A_1 r^2}{R^2}}) R^2 (2(2e^{\frac{A_1 r^2}{R^2}} r^2 - 5) \eta^2 + 3(2e^{\frac{A_1 r^2}{R^2}} r^2 \\
& - 5) \eta - 6))) \Big] \Big[ R^4 (8(e^{\frac{A_1 r^2}{R^2}} r^2 - 1) \eta^2 + 3(2e^{\frac{A_1 r^2}{R^2}} r^2 - 5) \eta - 6) (-2a^2 \eta \\
& \times (A_1 r^2 (8(8e^{\frac{2A_1 r^2}{R^2}} r^4 + 6e^{\frac{A_1 r^2}{R^2}} r^2 - 3) \eta^3 + (96e^{\frac{2A_1 r^2}{R^2}} r^4 + 68e^{\frac{A_1 r^2}{R^2}} r^2 - 61) \eta^2 \\
& + 12(3e^{\frac{2A_1 r^2}{R^2}} r^4 + 2e^{\frac{A_1 r^2}{R^2}} r^2 - 4) \eta - 12) - R^2 (4e^{\frac{2A_1 r^2}{R^2}} \eta (4\eta + 3)^2 r^4 - 4e^{\frac{A_1 r^2}{R^2}} \\
& \times (32\eta^3 + 84\eta^2 + 69\eta + 18) r^2 - 24\eta^3 - 61\eta^2 - 48\eta - 12)) r^4 + a(4e^{\frac{A_1 r^2}{R^2}} \\
& \times (11\eta^2 + 17\eta + 6) (e^{\frac{A_1 r^2}{R^2}} (2\eta^2 + 6\eta + 3) - 3(2\eta^2 + 3\eta + 1)) R^4 - A_1 \\
& \times (-4e^{\frac{A_1 r^2}{R^2}} \eta (148\eta^3 + 403\eta^2 + 339\eta + 90) r^2 + 4e^{\frac{2A_1 r^2}{R^2}} (2(70r^2 - 11) \eta^4 \\
& + 5(49r^2 - 20) \eta^3 + 3(43r^2 - 49) \eta^2 + 3(6r^2 - 29) \eta - 18) r^2 + 3(40\eta^4 \\
& + 179\eta^3 + 273\eta^2 + 168\eta + 36)) R^2 + 2A_1^2 r^2 \eta (8(8e^{\frac{2A_1 r^2}{R^2}} r^4 + 6e^{\frac{A_1 r^2}{R^2}} r^2 - 3) \eta^3 \\
& + (96e^{\frac{2A_1 r^2}{R^2}} r^4 + 68e^{\frac{A_1 r^2}{R^2}} r^2 - 61) \eta^2 + 12(3e^{\frac{2A_1 r^2}{R^2}} r^4 + 2e^{\frac{A_1 r^2}{R^2}} r^2 - 4) \eta - 12)) r^4 \\
& + R^2 (-A_1^2 (104\eta^4 + 363\eta^3 + 441\eta^2 - 4e^{\frac{A_1 r^2}{R^2}} r^2 (52\eta^3 + 123\eta^2 + 87\eta + 18) \eta \\
& + 216\eta + 4e^{\frac{2A_1 r^2}{R^2}} r^2 ((4r^2 - 22) \eta^4 + (23r^2 - 100) \eta^3 + 3(13r^2 - 49) \eta^2 \\
& + 3(6r^2 - 29) \eta - 18) + 36) r^4 - A_1 R^2 (104\eta^4 + 331\eta^3 + 381\eta^2 + 192\eta \\
& - 4e^{\frac{f r^2}{R^2}} r^2 (74\eta^4 + 141\eta^3 + 54\eta^2 - 33\eta - 18) + 4e^{\frac{2A_1 r^2}{R^2}} r^2 (4r^2 \eta^4 + 3(5r^2 \\
& - 22) \eta^3 + 9(r^2 - 15) \eta^2 - 87\eta - 18) + 36) r^2 + (-1 + e^{\frac{A_1 r^2}{R^2}}) R^4 \\
& \times (8(2e^{\frac{2A_1 r^2}{R^2}} r^4 - 26e^{\frac{A_1 r^2}{R^2}} r^2 + 13) \eta^4 + (60e^{\frac{2A_1 r^2}{R^2}} r^4 - 428e^{\frac{A_1 r^2}{R^2}} r^2 + 331) \eta^3
\end{aligned}$$

$$\begin{aligned}
& + \left( 36e^{\frac{2A_1r^2}{R^2}}r^4 - 300e^{\frac{A_1r^2}{R^2}}r^2 + 381\right)\eta^2 - 24\left(3e^{\frac{A_1r^2}{R^2}}r^2 - 8\right)\eta + 36)) \\
& \times \left\{ 2\left(-1 + e^{\frac{A_1r^2}{R^2}}\right)\left(\eta\left(2e^{\frac{A_1r^2}{R^2}}(\eta+3)r^2 - 13\eta - 17\right) - 6\right) + \frac{1}{R^4}\left\{ 2r^2 \right. \right. \\
& \times \left(-6a^2\eta^2r^2 + 6aA_1\eta^2r^2 - 4a^2\eta r^2 + 4aA_1\eta r^2 + 2e^{\frac{2A_1r^2}{R^2}}(a+A_1)R^2(\eta+1) \right. \\
& \times (11\eta+6)r^2 + 18aR^2 + 6A_1R^2 + 21aR^2\eta^2 + 13A_1R^2\eta^2 + 43aR^2\eta \\
& + 21A_1R^2\eta - e^{\frac{A_1r^2}{R^2}}(4a^2\eta(4\eta+3)r^4 + A_1R^2(2(\eta+2)(\eta+3)r^2 \\
& + (\eta+1)(11\eta+6)) + a(R^2(2(\eta(27\eta+29)+6)r^2 + (\eta+1)(11\eta+6)) \\
& \left. \left. \left. - 4A_1r^4\eta(4\eta+3))\right)\right)\right\} \right\}^{-1},
\end{aligned}$$

$$\begin{aligned}
\Gamma_t = & - \left[ 2(\eta+1)(A_1^2(2a\eta(8(2e^{\frac{fr^2}{R^2}}r^2 - 1)\eta^2 + 3(4e^{\frac{A_1r^2}{R^2}}r^2 - 5)\eta - 6)r^2 \right. \\
& + R^2(8(-18e^{\frac{A_1r^2}{R^2}}r^2 + e^{\frac{2A_1r^2}{R^2}}(10r^4 + r^2) + 9)\eta^3 + 3(-100e^{\frac{A_1r^2}{R^2}}r^2 \\
& + 4e^{\frac{2A_1r^2}{R^2}}(5r^2 + 2)r^2 + 77)\eta^2 + 6(-24e^{\frac{A_1r^2}{R^2}}r^2 + 2e^{\frac{2A_1r^2}{R^2}}r^2 + 39)\eta + 72))r^4 \\
& + A_1(-2a^2\eta(8(2e^{\frac{A_1r^2}{R^2}}r^2 - 1)\eta^2 + 3(4e^{\frac{A_1r^2}{R^2}}r^2 - 5)\eta - 6)r^4 - aR^2\eta(4e^{\frac{A_1r^2}{R^2}} \\
& \times \eta(4\eta+3)r^2 + 4e^{\frac{2A_1r^2}{R^2}}((4r^2 - 2)\eta^2 + 3(r^2 - 2)\eta - 3)r^2 - 3(8\eta^2 \\
& + 15\eta + 6))r^2 + R^4(-8(6e^{\frac{2A_1r^2}{R^2}}r^4 - 15e^{\frac{A_1r^2}{R^2}}r^2 + 7)\eta^3 - 3(-60e^{\frac{A_1r^2}{R^2}}r^2 \\
& + 4e^{\frac{2A_1r^2}{R^2}}(3r^2 - 2)r^2 + 51)\eta^2 + 12(5e^{\frac{A_1r^2}{R^2}}r^2 + e^{\frac{2A_1r^2}{R^2}}r^2 - 11)\eta - 36))r^2 \\
& + R^2(-2a^2\eta(8\eta^2 + 15\eta + 6)r^4 + 4ae^{\frac{A_1r^2}{R^2}}R^2\eta(e^{\frac{A_1r^2}{R^2}}(2\eta^2 + 6\eta + 3) \\
& - 3(2\eta^2 + 3\eta + 1))r^4 + (-1 + e^{\frac{A_1r^2}{R^2}})R^4(8(6e^{\frac{2A_1r^2}{R^2}}r^4 - 14e^{\frac{A_1r^2}{R^2}}r^2 + 7)\eta^3 \\
& + 9(4e^{\frac{2A_1r^2}{R^2}}r^4 - 20e^{\frac{A_1r^2}{R^2}}r^2 + 17)\eta^2 + (132 - 72e^{\frac{A_1r^2}{R^2}}r^2)\eta + 36)))(-a^2 \\
& \times (2e^{\frac{A_1r^2}{R^2}}r^2 + 1)\eta(4\eta+3)r^4 + a(A_1(2e^{\frac{A_1r^2}{R^2}}r^2 + 1)\eta(4\eta+3)r^2 + R^2(6e^{\frac{2fr^2}{R^2}} \\
& \times (2\eta^2 + 3\eta + 1)r^2 + 10\eta^2 + 21\eta - e^{\frac{A_1r^2}{R^2}}((28\eta^2 + 30\eta + 6)r^2 + 6\eta^2 \\
& + 9\eta + 3) + 9))r^2 + R^2(A_1(6e^{\frac{2A_1r^2}{R^2}}(2\eta^2 + 3\eta + 1)r^2 + 2\eta^2 + e^{\frac{A_1r^2}{R^2}}(r^2 \\
& \times (4\eta^2 - 6) - 3(2\eta^2 + 3\eta + 1)) - 3)r^2 + (-1 + e^{\frac{A_1r^2}{R^2}})R^2(2(2e^{\frac{A_1r^2}{R^2}}r^2
\end{aligned}$$

$$\begin{aligned}
& - 5)\eta^2 + 3(2e^{\frac{A_1 r^2}{R^2}} r^2 - 5)\eta - 6))) \Bigg] \Bigg[ (a^2 (R^2 (16(4e^{\frac{2A_1 r^2}{R^2}} r^4 - 8e^{\frac{A_1 r^2}{R^2}} r^2 + 3)\eta^4 \\
& + 2(48e^{\frac{2A_1 r^2}{R^2}} r^4 - 168e^{\frac{A_1 r^2}{R^2}} r^2 + 97)\eta^3 + 3(12e^{\frac{2A_1 r^2}{R^2}} r^4 - 92e^{\frac{A_1 r^2}{R^2}} r^2 + 93)\eta^2 \\
& - 24(3e^{\frac{A_1 r^2}{R^2}} r^2 - 7)\eta + 36) - A_1 r^2 (16(4e^{\frac{2A_1 r^2}{R^2}} r^4 - 6e^{\frac{A_1 r^2}{R^2}} r^2 + 3)\eta^4 + 2(48 \\
& \times e^{\frac{2A_1 r^2}{R^2}} r^4 - 140e^{\frac{A_1 r^2}{R^2}} r^2 + 97)\eta^3 + 9(4e^{\frac{2A_1 r^2}{R^2}} r^4 - 28e^{\frac{A_1 r^2}{R^2}} r^2 + 31)\eta^2 \\
& - 24(3e^{\frac{A_1 r^2}{R^2}} r^2 - 7)\eta + 36)) r^4 + a(4e^{\frac{A_1 r^2}{R^2}} \eta(\eta + 1)(e^{\frac{A_1 r^2}{R^2}} (2\eta^2 + 6\eta + 3) \\
& - 3(2\eta^2 + 3\eta + 1)) R^4 - A_1 (8(-46e^{\frac{A_1 r^2}{R^2}} r^2 + e^{\frac{2A_1 r^2}{R^2}} (26r^2 - 1)r^2 + 21)\eta^4 \\
& \times (-980e^{\frac{A_1 r^2}{R^2}} r^2 + 4e^{\frac{2A_1 r^2}{R^2}} (79r^2 - 8)r^2 + 651)\eta^3 + 12(-68e^{\frac{A_1 r^2}{R^2}} r^2 \\
& + e^{\frac{2A_1 r^2}{R^2}} (10r^2 - 3)r^2 + 75)\eta^2 - 6(36e^{\frac{A_1 r^2}{R^2}} r^2 + 2e^{\frac{2A_1 r^2}{R^2}} r^2 - 87)\eta + 108) R^2 \\
& + a^2 r^2 (16(4e^{\frac{2A_1 r^2}{R^2}} r^4 - 6e^{\frac{A_1 r^2}{R^2}} r^2 + 3)\eta^4 + 2(48e^{\frac{2A_1 r^2}{R^2}} r^4 - 140e^{\frac{A_1 r^2}{R^2}} r^2 + 97)\eta^3 \\
& + 9(4e^{\frac{2A_1 r^2}{R^2}} r^4 - 28e^{\frac{A_1 r^2}{R^2}} r^2 + 31)\eta^2 - 24(3e^{\frac{A_1 r^2}{R^2}} r^2 - 7)\eta + 36)) r^4 + R^2 (A_1^2 \\
& \times (8(-2e^{\frac{A_1 r^2}{R^2}} r^2 + e^{\frac{2A_1 r^2}{R^2}} (2r^4 + r^2) + 1)\eta^4 + (-108e^{\frac{A_1 r^2}{R^2}} r^2 + 4e^{\frac{2A_1 r^2}{R^2}} \\
& \times (11r^2 + 8)r^2 + 63)\eta^3 + 12(-14e^{\frac{A_1 r^2}{R^2}} r^2 + e^{\frac{2A_1 r^2}{R^2}} (2r^2 + 3)r^2 + 12)\eta^2 \\
& + 6(-12e^{\frac{A_1 r^2}{R^2}} r^2 + 2e^{\frac{2A_1 r^2}{R^2}} r^2 + 21)\eta + 36) r^4 + A_1 R^2 \eta (8\eta^3 + 31\eta^2 + 36\eta \\
& - 4e^{\frac{A_1 r^2}{R^2}} r^2 (2\eta^3 + 9\eta^2 + 9\eta + 3) + 4e^{\frac{2A_1 r^2}{R^2}} r^2 (4r^2 \eta^3 + 3(r^2 + 2)\eta^2 + 9\eta + 3) \\
& + 12)r^2 - (-1 + e^{\frac{A_1 r^2}{R^2}}) R^4 \eta (8(2e^{\frac{2A_1 r^2}{R^2}} r^4 - 2e^{\frac{A_1 r^2}{R^2}} r^2 + 1)\eta^3 + (12e^{\frac{2A_1 r^2}{R^2}} r^4 \\
& - 44e^{\frac{A_1 r^2}{R^2}} r^2 + 31)\eta^2 + (36 - 24e^{\frac{A_1 r^2}{R^2}} r^2)\eta + 12)) (-2a^2 \eta (2e^{\frac{A_1 r^2}{R^2}} (4\eta + 3)r^2 \\
& + 3\eta + 2) r^4 + a(2A_1 \eta (2e^{\frac{A_1 r^2}{R^2}} (4\eta + 3)r^2 + 3\eta + 2) r^2 + R^2 (2e^{\frac{2A_1 r^2}{R^2}} (11\eta^2 \\
& + 17\eta + 6) r^2 + 21\eta^2 + 43\eta - e^{\frac{A_1 r^2}{R^2}} (2(27\eta^2 + 29\eta + 6) r^2 + 11\eta^2 + 17\eta + 6) \\
& + 18)) r^2 + R^2 (A_1 (2e^{\frac{2A_1 r^2}{R^2}} (11\eta^2 + 17\eta + 6) r^2 + 13\eta^2 + 21\eta - e^{\frac{A_1 r^2}{R^2}} (2(\eta^2 \\
& + 5\eta + 6) r^2 + 11\eta^2 + 17\eta + 6) + 6) r^2 + (-1 + e^{\frac{A_1 r^2}{R^2}}) R^2 ((2e^{\frac{A_1 r^2}{R^2}} r^2 \\
& - 13)\eta^2 + (6e^{\frac{A_1 r^2}{R^2}} r^2 - 17)\eta - 6))) \Bigg].
\end{aligned}$$

## Appendix C:

The comprehensive table of symbols is given as follows.

Table 3: Definitions and first appearances of symbols used in the manuscript.

Symbol	Meaning	Context	First Appearance
$\mathcal{Q}$	Non-metricity scalar	Measures deviation from metricity	Abstract
$\mathbb{T}$	Trace of the energy-momentum tensor	Summarizes matter contribution	Abstract
$\mathcal{Q}_{\rho\xi\mu}$	non-metricity tensor	Describes geometric deformation	Eq.(3)
$P_{\rho\xi\mu}$	Superpotential related to non-metricity	Derived from non-metricity contributions	Eq.(14)
$f(\mathcal{Q}, \mathbb{T})$	An arbitrary function of $\mathcal{Q}$ and $\mathbb{T}$	Governs the dynamics of the gravity model	Abstract
$L_m$	Matter Lagrangian	Represents matter content	Eq.(9)
$\sigma = P_t - P_r$	Anisotropy factor	Quantifies the pressure anisotropy	Eq.(21)
$\zeta, \eta$	Parameters in $f(\mathcal{Q}, \mathbb{T})$	Coupling constants linking gravity and matter	Eq.(27)
$A_1, a_1, a$	Krori-Barua metric parameters	Define the metric potentials $\alpha(r), \beta(r)$	Eq.(31)
$u$	Compactness parameter	Relates mass to radius: $u = \frac{2M}{R}$	Eq.(36)
$v_r^2, v_t^2$	Radial and tangential sound speeds	Measure sound propagation speeds	Eq.(42)

**Data availability:** No new data were generated or analyzed in support of this research.



## References

- [1] Perlmutter, S. et al.: *Astrophys. J.* **517**(1999)565.
- [2] Spergel, D.N. et al.: *Astrophys. J. Suppl. Ser.* **148**(2003)175.
- [3] Bennett, C.L. et al.: *Astrophys. J. Suppl. Ser.* **148**(2003)97.
- [4] Nojiri, S. and Odintsov, S.D.: *Phys. Rev. D* **68**(2003)123512.
- [5] Weyl, H.S.: *Preuss. Akad. Wiss.* **1**(1918)465.
- [6] Nester, J.M. and Yo, H.J.: *Chin. J. Phys.* **37**(1999)113.
- [7] Jimenez, J.B., Heisenberg, L. and Koivisto, T.: *Phys. Rev. D* **98**(2018)044048.
- [8] Lazkoz, R. et al.: *Phys. Rev. D* **100**(2019)104027.
- [9] Mandal, S., Sahoo, P.K. and Santos, J.R.: *Phys. Rev. D* **102**(2020)024057.
- [10] Shekh, S.H.: *Phys. Dark Univ.* **33**(2021)100850.
- [11] Lin, R.H. and Zhai, X.H.: *Phys. Rev. D* **103**(2021)124003.
- [12] Frusciante, N.: *Phys. Rev. D* **103**(2021)044021.
- [13] Esposito, F. et al.: *Phys. Rev. D* **105**(2022)084061.
- [14] Dimakis, N. et al.: *Phys. Rev. D* **106**(2022)043509.
- [15] Sokoliuk, O. et al.: *Mon. Not. R. Astron. Soc.* **522**(2023)252.
- [16] Bhar, P. and Pretel, J.M.: *Phys. Dark Univ.* **42**(2023)101322.
- [17] Khyllep, W. et al.: *Phys. Rev. D* **107**(2023)044022; Koussour, M. et al.: *Prog. Theor. Exp. Phys.* **2023** (2023)113E01; Gadbail, G.N., Mandal, S. and Sahoo, P.K.: *Astrophys. J.* **972**(2024)174.
- [18] Sharif, M. and Ajmal, M.: *Chin. J. Phys.* **88**(2024)706.
- [19] Sharif, M., Gul, M.Z. and Fatima, N.: *New Astron.* **109**(2024)102211.

- [20] Xu, Y. et al.: Eur. Phys. J. C **79**(2019)708; **80**(2020)449.
- [21] Arora, S. et al.: Phys. Dark. Universe **30**(2020)100664.
- [22] Bhattacharjee, S. and Sahoo, P.K.: Eur. Phys. J. C **80**(2020)289.
- [23] Godani, N. and Samanta, G.C.: Int. J. Geom. Methods Mod. Phys. **18**(2021)2150134.
- [24] Agrawal, A.S. et al.: Phys. Dark Univ. **33**(2021)100863.
- [25] Shiravand, M., Fakhry, S. and Farhoudi, M.: Phys. Dark Univ. **37**(2022)101106.
- [26] Nájera, A. and Fajardo, A.: J. Cosmol. Astropart. Phys. **2022**(2022)020.
- [27] Lalke, A.R., Singh, G.P. and Singh, A.: Int. J. Geom. Methods Mod. Phys. **20**(2023)2350131.
- [28] Tayde, M., Hassan, Z. and Sahoo, P.K.: Phys. Dark Univ. **42**(2023)101288.
- [29] Khurana, M. et al.: Phys. Dark Universe **43**(2024)101408.
- [30] Sharif, M. and Ibrar, I.: Chin. J. Phys. **89**(2024)1578.
- [31] Sharif, M. and Ibrar, I.: Eur. Phys. J. Plus **139**(2024)1.
- [32] Sharif, M. and Ibrar, I.: Phys. Scr. **99**(2024)105034.
- [33] Sharif, M. and Ibrar, I.: Chin. J. Phys. **92**(2024)333.
- [34] Ibrar, I and Sharif, M.: Nucl. Phys. B **1011**(2025)116791.
- [35] Ibrar, I and Sharif, M.: Astron. Comput. **53**(2025)100967.
- [36] Sharif, M. et al.: Pramana **99**(2025)56.
- [37] Sharif, M. and Ibrar, I.: Nucl. Phys. B **1015**(2025)116896.
- [38] Baade, W. and Zwicky, F.: Phys. Rev. **46**(1934)76.
- [39] Longair, M.S.: *High Energy Astrophysics* (Cambridge University Press, 1994).

- [40] Zand, J.I.T. et al.: Astron. Astrophys. **345**(1999)100.
- [41] van Kerkwijk, M.H. et al.: Astrophys. J. **563**(2001)41.
- [42] Markwardt, C.B. and Swank, J.H.: The Astronomers' Telegram **495**(2005)1.
- [43] Patruno, A. et al.: The Astronomers' Telegram **2407**(2010)1.
- [44] Mak, M.K. and Harko, T.: Int. J. Mod. Phys. D **13**(2004)156.
- [45] Kramer, M. et al.: Science **314**(2006)97.
- [46] Sharma, R. et al.: Mon. Not. R. Astron. Soc. **492**(2020)4361.
- [47] Nashed, G.G.L.: Eur. Phys. J. C **83**(2023)698.
- [48] Nashed, G.G.L. and Capozziello, S.: Eur. Phys. J. C. **84**(2024)17.
- [49] Dirac, P.A.M.: Proc. R. Soc. Lond. A **333**(1973) 403.
- [50] Landau, L.D. and Lifshitz, E.M.: *The Classical Theory of Fields* (Elsevier, 2013).
- [51] Xu, Y. et al.: Eur Phys. J. C **79**(2019)19.
- [52] Xu, Y. et al.: Eur Phys. J. C **80**(2020)22; Tayde, M. et al.: Chin. Phys. C **46**(2022)115101.
- [53] Krori, K.D. and Barua, J.: J. Phys. A **8**(1975)508.
- [54] Bhar, P. et al.: Eur Phys. J. C **83**(2023)1.
- [55] Özel, F., Güver, T. and Psaltis, D.: Astrophys. J. **693**(2009)1775.
- [56] Deb, D. et al.: Ann. Phys. **387**(2017)239.
- [57] Ivanov, B.V.: Phys. Rev. D **65**(2002)104011.
- [58] Barraco, D.E., Hamity, V.H. and Gleiser, R.J.: Phys. Rev. D **67**(2003)064003.
- [59] Böhmer, C., Harko, T.: Class. Quantum Grav. **23**(2006)6479.

- [60] Zeldovich, Y.B. and Novikov, I.D.: *Relativistic Astrophysics. Vol. 1: Stars and Relativity* (Univ. Chicago Press, Chicago, 1971).
- [61] Abreu, H. et al.: *Class. Quantum Grav.* **24**(2007)4631.
- [62] Herrera, L.: *Phys. Lett. A* **165**(1992)206.
- [63] Chandrasekhar, S.: *Astrophys. J.* **140**(1964)417.
- [64] Chan, R., Herrera, L. and Santos, N.: *Mon. Not. R. Astron. Soc.* **265**(1993)533.
- [65] Heintzmann, H. and Hillebrandt, W.: *Astron. Astrophys.* **38**(1975)51.
- [66] Tolman, R.C.: *Phys. Rev.* **35**(1930)896.
- [67] Tolman, R.C.: *Phys. Rev.* **55**(1939)364.
- [68] Oppenheimer, J.R. and Volkoff, G.M.: *Phys. Rev.* **55**(1939)374.
- [69] Shamir, M.F. and Zia, S.: *Eur. Phys. J. C* **77**(2017)448.
- [70] Singh, K.N. et al.: *Eur. Phys. J. A* **53**(2017)21.
- [71] Buchdahl, A.H.: *Phys. Rev. D* **116**(1959)1027.